REPORT DOCUMENTATION PAGE

Form Approved
OMB NO. 0704-0188

1. AGENCY USE ONLY (Leave Blank)	2. REPORT DATE	3. REPORT TYPE AND DATES COVERED
	July 29, 2004	Final Report 01 Apr 01 , to December 31, 2003

4. TITLE AND SUBTITLE
A fundamental investigation into the deformation and failure behavior of heterogeneous materials with the aim of developing design guidelines

5. FUNDING NUMBERS
DAAD19-01-1-0487

6. AUTHOR(S)
Krishnaswamy RAVI-CHANDAR

7. PERFORMING ORGANIZATION NAME(S) AND ADDRESS(ES)
Center for Mechanics of Solids Structues and Materials
University of Texas at Austin
Austin, TX 78712-1085

8. PERFORMING ORGANIZATION REPORT NUMBER

9. SPONSORING / MONITORING AGENCY NAME(S) AND ADDRESS(ES)
U. S. Army Research Office
P.O. Box 12211
Research Triangle Park, NC 27709-2211

10. SPONSORING / MONITORING AGENCY REPORT NUMBER
42304.1-EG

11. SUPPLEMENTARY NOTES
The views, opinions and/or findings contained in this report are those of the author(s) and should not be construed as an official Department of the Army position, policy or decision, unless so designated by other documentation.

12 a. DISTRIBUTION / AVAILABILITY STATEMENT
Approved for public release; distribution unlimited.

12 b. DISTRIBUTION CODE

13. ABSTRACT (Maximum 200 words)

Using the biomimetic idea of gradual changes in the orientation of subsequent layers in fiber reinforced materials, we have developed a helicoidal composite material. In this material, the orientation in each subsequent layer is changed only by 10 degrees; this results in a graded composite material, with significantly reduced interlaminar shear stresses that drive delamination. The mechanisms of failure has been investigated; the material is shown to possess superior mechanical properties under both static and dynamic loading conditions.

14. SUBJECT TERMS	15. NUMBER OF PAGES
	66
	16. PRICE CODE

17. SECURITY CLASSIFICATION OR REPORT	18. SECURITY CLASSIFICATION ON THIS PAGE	19. SECURITY CLASSIFICATION OF ABSTRACT	20. LIMITATION OF ABSTRACT
UNCLASSIFIED	**UNCLASSIFIED**	**UNCLASSIFIED**	**UL**

1. **List of Manuscripts**

   T. Apicharttabrut and K. Ravi-Chandar, Development of a helicoidal architecture for optimized mechanical response of a composite, under preparation.

   D. Bonamy and K. Ravi-Chandar, Interaction of propagating cracks with shear waves, Physical Review Letters, 91, 2003.

2. **Scientific Personnel**

   Professor K. Ravi-Chandar, Principal Investigator, Mr. Terapat Apicharttabrut, Graduate Student, Dr. Daniel Bonamy, Research Associate.

3. **Report of Inventions**

   There are no inventions to report.

4. **Scientific progress and accomplishments**

   The scientific progress and accomplishments are described in the following pages.

5. **Technology transfer**

   We have been in contact with Dr. Alex Hsieh of ARL regarding the confined compression experiments reported in the previous interim progress report. It appears that the idea has merit in transparent armor, where the application of residual compression can reduce cracking due to loading; some preliminary tests have been performed on PMMA plates with confinement that demonstrate elimination of lateral and radial cracks. We are pursuing this further to establish parameters for experiments; this will be done in collaboration with Dr. Stephen Bless of the Institute for Advanced technology at the University of Texas at Austin.
   We have also contacted with the group of Dr. Chris Hoppel about the use of the helicoidal composites in high performance applications in the Army.

TABLE OF CONTENTS

LIST OF FIGURES iv

LIST OF TABLES vi

1. INTRODUCTION 1

2. DESIGN OF THE HELICOIDAL COMPOSITE 9

    2.1. Helicoidal Architecture 11

    2.2. Processing Induced Residual Stresses 15

    2.3. Through-Thickness Reinforcement 17

        2.3.1. The Three Point Bending Test 21

        2.3.2. The Double Cantilever Beam Test: 24

3. FABRICATION OF HELICOIDAL COMPOSITES 31

4. MECHANICAL CHARACTERIZATION OF THE HELICOIDAL COMPOSITE 36

    4.1. Uniaxial Tension Test 36

    4.2. Failure Mechanisms in the Helicoidal Composite under Uniaxial Tension 39

    4.3. Plate Bending Test 42

    4.4. Impact Tests 51

5. CONCLUSION 55

6. REFERENCES 57

LIST OF FIGURES

Figure 1.	Structure of osteons in mammalian bones (Reproduced from Neville, 1993).	8
Figure 2.	Orientation of the layers of the helicoidal composite	12
Figure 3.	Reduced stiffness matrix of the laminate as a function of orientation with respect to the global x-direction.	14
Figure 4.	Residual stress distribution in the helicoidal specimen	16
Figure 5.	A close-up view of the staple-pin used for thickness reinforcement	20
Figure 6.	Load-Displacement Variation for the Three Point Bending Test	23
Figure 7.	The reinforcement pattern for the DCB specimen (top view)	25
Figure 8.	Double cantilever beam specimen test for the determination of the interlaminar fracture toughness	26
Figure 9.	Variation of the load with crack opening displacement for the DCB test.	27
Figure 10.	Variation of the fracture toughness K_I/K_{IC} and crack length (staple-reinforced specimen)	30
Figure 11.	Staple-reinforced circular plate prior to curing	30
Figure 12.	Temperature and pressure cycle used for curing the helicoidal composite	32
Figure 13.	Location of the thermocouples for evaluation of the through-thickness temperature distribution	33
Figure 14.	Through-thickness temperature distribution in the specimen during curing.	34
Figure 15.	Results of uniaxial tension tests on uniaxial, ±45° and helicoidal specimens.	38
Figure 16.	The failure pattern of helicoidal composite specimen under uniaxial tension. The arrows drawn suggest that in successive planes, the fracture propagated along different planes and directions	40

Figure 17. The failure mechanism of helicoidal composite specimen under uniaxial tension. Multiple matrix cracks in different layers are shown. A schematic diagram of the overall development of matrix cracks is shown to the right of the photographs 41

Figure 18. Plate bending test. The composite specimen is clamped between two thick aluminum plates and bolted down. A steel ball attached to a ram is used to apply the load at the center of the plate 43

Figure 19. Load and Displacement Relationship for the Circular Plate Bending Test 49

Figure 20. Damage patterns observed in the circular plate test. (a) 0° specimen. (b) and (c) Top and bottom sides of the ±45°, (d) and (e) top and bottom sides of the helicoidal specimen, (f) and (g) reinforced helicoidal specimen 50

Figure 21. Impact test arrangement. Striker used in the impact tests is shown on the right. Conical tip was made of steel and the pusher was made of polycarbonate. Diameter 2 in 52

Figure 22. Back side of the ±45º specimen after the impact test 53

Figure 23. (a) and (b) Impact side of the helicoidal specimen after the impact test; the impact speed was 55 m/s. (c) Thickness section of the plate showing localized damage at the impact point and delamination along a specific layer 54

LIST OF TABLES

Table 1. NCT304-1 Carbon/Epoxy property 13

Table 2. Maximum load and deflection in the different specimens 48

1. INTRODUCTION

The mechanisms of deformation and failure of composites have been investigated extensively, by a number of investigators for different composite material systems over a long period of time. Many of the essential mechanisms of deformation and damage have long been identified (see for instance, Hull, 1981): transverse matrix cracks, fiber breaks, interface cracks, delamination, microbuckling, kink bands and other forms of damage arise in composite materials. All of these have been studied in different model systems and appear to be fairly well understood at least phenomenologically. The big question is the following: *how does one translate this into design guidelines for use by practicing engineers*? In addressing this issue it is important to distinguish between the stiffness and strength; it appears that stiffness can be determined fairly easily from the properties of the constituents whereas the problem of strength is still unresolved. On the other hand, according to MIL-HDBK-17-3E, "it may be desirable to regard the strength of a unidirectional fiber composite subjected to a single principal stress component as a quantity to be measured experimentally, rather than deduced from constituent properties." In guidelines developed for use of composites in engineering applications, such as the MIL Handbook as well as other sources (Pilato and Michno, 1994, Swanson, 1997), composites have been treated as materials with characteristic properties that can be determined in standard tests and then incorporated in designs in much the same way as the more traditional homogenous materials. Thus, in incorporating the knowledge of the deformation and failure mechanisms into practice, the current methodology is to provide a number of *ad hoc* "strengths" – such as the tension strength (ASTM D 3039), compression strength (ASTM D 695), open-hole tension strength, open-hole compression

strength (NASA 1092 specification), edge delamination strength (O'Brien 1982), compression after impact strength etc. We note that none of these is a real material property – they are material system, and geometry dependent. For instance, the open-hole compression strength must be determined not only for the particular set of constituents, and particular lay-up, but also for the specific hole size! The use of such ad hoc strengths is an implicit recognition of the fact that these strengths are not material properties but that they depend on the geometry of the component, the lay-up of the laminates, and the loading conditions that influence the deformation and failure modes that become operational. In other words, there is a significant interaction between the material constituents (heterogeneity) and the structure.

Another question that is perhaps far more important and overreaching in its impact pertains to design philosophy. Why should we use the methodologies developed for homogeneous materials to design with heterogeneous materials? This is best illustrated with a few examples. First, consider beams made of composite materials. The evolution of the I-beam is well suited to homogeneous materials; the flanges take tensile and compressive stresses while the web is effective in carrying shear stresses. The highlight of such a concept is, of course, the diagonal-tension beam, where the web thickness is so small that wrinkles form along the compression diagonals and the shear in the web is taken only in the form of tension. So, even in designing with homogeneous materials, ingenious ideas contribute to optimizing the structural capability. Composites offer ever more possibilities in this direction; however, typical composite structural elements have been designed from a manufacturability perspective, regardless of the mechanical penalty. Lay-up of unidirectional prepregs has been the preferred route to the fabrication of most composite structures,

although three-dimensional woven composites have become more popular recently. Composite materials fabricated in this way are typically shear and compression strength limited. Two possibilities can be explored: first, is it possible to design a suitable geometrical arrangement of the constituents to exploit the high tensile strength of composites? In other words, what is the design equivalent to the I-beam or diagonal-tension beam when stiffness and strength are anisotropic and heterogeneous? The second possibility: are there design options for pre-stressing the structure (again anisotropically in the heterogeneous medium) in such a way that the strength differential effects (between tension, shear and compressive modes as well as other modes such as edge-delamination mode) are exploited to the fullest extent possible. These questions indicate the intricate interconnectedness between structural design and mechanics analysis on the one hand, and the composite material design and manufacturing considerations on the other.

The second example is that of joining: two types of joints – adhesive and mechanically fastened – are typically used in joining composites. Mechanically fastened joints are preferred in locations where high load transfer is to be accomplished. Given that holes and cut-outs cause stress concentrations just as in the case of structures made of homogeneous materials, but also that due to the anisotropy and heterogeneity the problems are exacerbated in composites, are holes and cut-outs desirable or necessary? This approach to joining arises once again simply by adopting ideas suitable for ductile homogeneous materials. While introducing holes in homogeneous materials does nothing to the "strength of the material", the situation is quite different in composites. The simple operation of making a hole introduces discontinuities in the phase geometries of the constituents, introduces free ends

and downgrades the "strength" of the material; thus the plethora of ad hoc strengths. In addition, the strength also depends on the hole-diameter and the nature of loading – uniaxial tension, compression, biaxial, shear etc. The approach taken for fiber dominated failure is due to Whitney and Nuismer (1974): a ply-level failure criterion is evaluated at a characteristic distance d_0 from the hole. d_0 is a function of the lamina properties, lay-up, as well as the loading condition and is obtained by correlating the unnotched and open hole strengths. Clearly the approach has been to regard the problem as one where the material is taken to dictate the strength and the structure is analyzed to evaluate the onset of failure; why not examine the fastening process? Are there ways of introducing holes without introducing damage to the fibers, matrix and the interfaces – in other words, integrating structural and material design across the microstructural and macroscopic length scales.

Current trends in composite structure design may be characterized as a sequential relationship between material design and structure design. The traditional triad in materials science is the interaction between the processing, microstructure and mechanical properties. This occurs completely independently of the final structural configuration. Within the domain of structural design, the "allowable" mechanical properties are derived from the materials designer and simply used in the design and analysis of reliability of the structure. Some weak feedback on manufacturability concerns may occur between the structural designer and the materials designer. The length scales that the two groups handle are simply far too different and are assumed not to interact. This sequential procedure has worked quite well in the case of homogeneous, isotropic materials. However, the situation is quite different for heterogeneous materials.

One of the main approaches to the development of guiding principles for generalization has been the use of micromechanics. The main idea is to identify the appropriate deformation and/or failure mechanisms, to incorporate this into a continuum analysis of a representative volume element or a representative unit cell, and then to recover a "homogenized" material property for that particular deformation or failure mode. This approach provides a prediction of the properties of the composites with known phase geometry; in general, the determination of the stiffness properties is accomplished satisfactorily. On the other hand, determination of strength is fraught with problems. First, the *in situ* properties of the constituents could be quite different from the bulk properties; while this is well-recognized (see for instance, Bahei-El-Din and Dvorak, 1980), there has not been much effort in addressing these differences. Secondly, the interfacial bonds are typically not well characterized in terms of their failure behavior and this influences the predictions of homogenized properties significantly. Furthermore, micromechanics models are inherently nonunique in the sense that more than one assumed micromechanical model can provide the same homogenized prediction; thus scalability or transferability of the results from one structure to another and one scale to another becomes a significant problem. Generalization of micromechanically determined material properties to multiaxial loading states is also a hurdle that has not yet been overcome.

An alternate approach is one where the composite is considered to be a homogeneous, anisotropic continuum and its response to loading is measured experimentally at the macroscopic scale. This approach to characterizing the inelastic response of composites is reviewed by Sun, (1993). It is a purely phenomenological theory and must rely on extensive

experimental characterization of the properties for each particular implementation of the composite material. In some sense, the use of ad hoc strengths discussed earlier is the basis of this approach. The number of tests required to characterize such "strengths" and qualify the material is quite large. "A total of 395 tests are specified if only one laminate thickness and one fastener head style are required to cover application design variables" (MIL Handbook-17-1E, p.2-65). Also, since the role of the heterogeneity is considered only in the average sense, it becomes difficult to develop materials design guidelines. Experiments designed to determine the macroscopic properties are not necessarily "clean" experiments; examining the literature in compressive and shear strengths, one could easily identify differences in opinion amongst different investigators. A recent review of the compression strength testing for thick composites contains about three hundred references (Schultheisz and Waas, 1996 and Waas and Schultheisz, 1996) dealing with this issue; many different phenomenological and micromechanical models have been used. Generalization of these ideas to multiaxial stress states has not been demonstrated, although some recent progress has been made by Kyriakides *et al*, (1995), who did not use a homogenization approach, but rather modeled the heterogeneity completely in a numerical simulation. In determining the shear behavior of composites, according to the MIL-Handbook-17-IE, p.6-70) "i.) there are no standard (or nonstandard) test methods that are capable of producing a perfectly pure shear stress condition to failure for every material, ii) the strengths resulting from test methods that do not consistently produce reasonable approximation of pure shear, or that cause failure by a non-shear failure mode, should not be termed shear strength". Lessard *et al*., (1997), have

tabulated 31 different test configurations for determining the shear response of composites. Thus, the evaluation of the shear behavior is still an unresolved problem.

In this research the behavior of a carbon/epoxy composite material is examined. Generally, the fiber directions of laminated composites are changed abruptly to the 0°, 30°, 45° and 90° directions; therefore the interlaminar shear stress – one of the major causes of the delamination – arises from the elastic properties mismatch between each layer. Minimization of this interlaminar shear stress should result in suppressing the tendency for the development of delamination. While a straightforward stress analysis using classical lamination theory will be used to determine these interlaminar shear stresses, some guidance on the appropriate design of the lamination can be obtained quickly from biological fibrous composites. Neville (1993) describes the structure and properties of such composites; in particular, the orientation change between neighboring layers of unidirectional fibers is typically on the order of 10° to 20°. Giraud-Guille (1988) examined the osteons in mammalian bones; these are concentric cylinders in which collagen fibers are arranged in specific directions. Giraud-Guille found two types of arrangements as shown in Figure 1. In the first type, orientation of the collagen fibers in each successive layer exhibited an orientation change of 90°. In the second type, called ***helicoidal***, the change in orientation between neighboring layers was in the range of 10° to 20°. Of course, in the mammalian bone, many such osteons are cemented together to form a haversian system and a much more complex macrostructure. Therefore, drawing on the biological experience, we developed the helicoidal architecture to build a laminated carbon-fiber epoxy-matrix composite. However, since interlaminar strength is still governed by the matrix material, the delamination

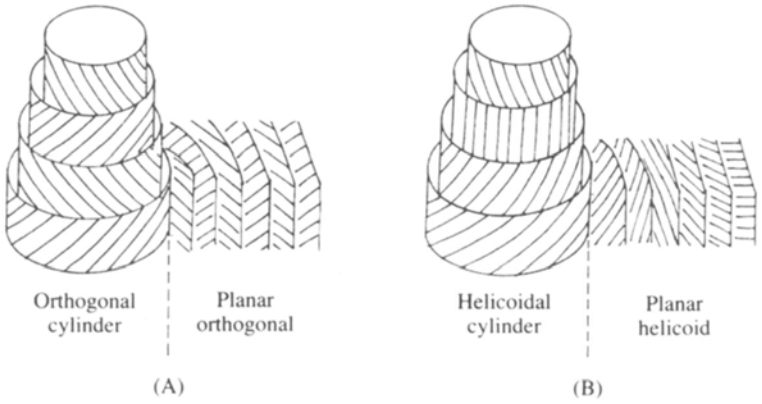

Figure 1. Structure of osteons in mammalian bones (Reproduced from Neville, 1993).

resistance must be increased by using through-thickness reinforcement (Barrett, 1996; Rugg *et al*., 1998, 2002; Mouritz *et al*., 1997a, 1999); these reinforcements increase the load capacity, and prevent initiation and propagation of delamination cracks. The z-stapling reinforcement with an appropriate pattern was evaluated and implemented in this work as described in detail later in this report. The resulting helicoidal composite exhibits significantly improved mechanical properties.

This report is organized as follows. In Section 4.2, we describe the design of the helicoidal composite and its through-thickness reinforcement. Procedures for the lay-up, stapling reinforcement, curing and specimen preparation are discussed in detain in Section 4.3. The response of the helicoidal composite and comparison to classical laminations under uniaxial tension, three-point bending and plate bending loading conditions are presented in Section 4.4. The impact response of the helicoids is also compared to that of the classical

lamination in this section; the superior performance of the helicoids under impact loading conditions suggests that minimizing the interlaminar shear stresses is important in improving the strength and toughness of fiber reinforced materials. Finally, suggestions for further development of the helicoidal composite are discussed in the concluding section.

2. DESIGN OF THE HELICOIDAL COMPOSITE

Interlaminar stresses are a major cause of delamination in composites. This is especially true when the specimen lay-up contains layers with abrupt changes in the fiber direction. Christensen and DeTeresa (1992) showed that the edge singularities that arise in laminated composites either vanish or are minimized for certain special laminations. This is a very interesting observation but only applies for special orientations of the loading; however, the underlying idea that through proper choice of fiber architecture one may influence the development of damage in composite materials is a very important one as we discuss later. This idea has been followed up in many analytical investigations, but to our knowledge, not in experimental investigations. More recently, Suvorov and Dvorak (2001a) have explored the possibility of prestressing selected lamina in order to control the development of free-edge stresses; this is somewhat akin to prestressing concrete with rebar, with the additional influence of material anisotropy. They suggest that by selectively prestressing certain layers prior to matrix infiltration/consolidation and then releasing upon curing, large compressive prestress can be generated in the matrix layers thereby minimizing matrix cracking and delamination. Sovorov and Dvorak (2001b) also indicate that designs of such prestressed laminate/ceramic plate assembly can also introduce significant compressive stresses of the order of 600 MPa to 1 GPa in the ceramic layer. These models raise interesting possibilities for enhancing the mechanical properties of composite materials; the helicoidal composite is a development along these lines. The helicoidal architecture, motivated by biological observations and simply by the fact that property gradation must decrease the interlaminar

shear stresses, offers the possibility of improved material properties. In this section, we discuss considerations in the design of the helicoids.

2.1. Helicoidal Architecture

Since the design parameter space – of material properties, property gradation, residual and pre-stress etc – is quite large, we approached the design from a geometric perspective. Considering only a plate structure, limiting the thickness to a nominal 0.25 in, and using standard prepregs, the starting parameters of the design of the helicoids were well constrained. Limiting the plate thickness to 0.25 *in* enabled experimental comparison to other graphite-epoxy plates of classical lamination architectures. Within these constraints, we have potentially 40 layers to distribute across the plate thickness. Taking a cue from biological composites, if we use an orientation change of 10° between neighboring layers, two pitches of a helix can be described in 36 layers. The additional 4 layers were placed in middle, all oriented in the 0° direction; in applications, this may be taken as the direction of the most common loading. In order to eliminate or minimize the elastic coupling between extension, bending and twisting deformations, we attempted to enforce symmetry and balance of the lamination about the middle plane of the plate. Both symmetry and balance can be accommodated by using the following graded architecture for the lamination sequence: $[180/170/160/150/140/130/120/110/100/90/80/70/60/50/40/30/20/10/(0)2]_s$. This gradation in the orientation of the fibers in the helicoidal composite is shown in Figure 2. Clearly, there are many other possible options for the lamination, and an optimization of the orientation

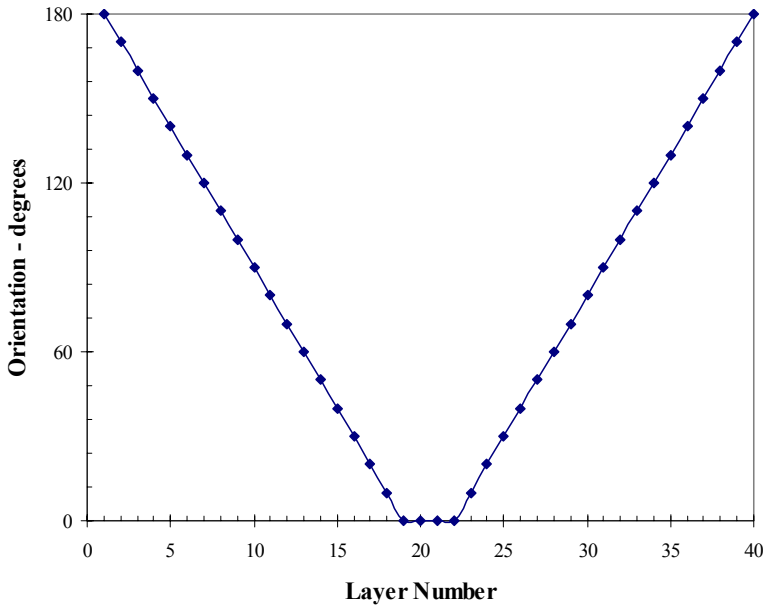

Figure 2. Orientation of the layers of the helicoidal composite.

needs to be evaluated. It is also possible to consider specific layups for each particular application. This was not addressed in the current research program.

The pre-pregs are carbon-epoxy rolls obtained from Newport Adhesives and Composites (designation NCT 304-1). The nominal properties of this material are listed in Table 1. The properties of the prepregs assumed in our analysis are given below:

$$E_1 = 124\,\text{GPa}, E_2 = 12.5\,\text{GPa}, G_{12} = 4.4\,\text{GPa}, \nu_{12} = 0.303, \nu_{21} = 0.03 \qquad (1)$$

For the 40 layer lamination described above, the laminate stiffness matrix is easily calculated and is shown below:

$$\mathbf{A} = \begin{bmatrix} 493 & 116 & 0 \\ 116 & 359 & 0 \\ 0 & 0 & 121 \end{bmatrix} \times 10^6 \text{ N/m}, \ \mathbf{B} = 0, \ \mathbf{D} = \begin{bmatrix} 2000 & 491 & -424 \\ 491 & 1370 & -259 \\ -424 & -259 & 512 \end{bmatrix} \text{N/m} \qquad (2)$$

The fact that all components of the **B** matrix are zero could have been guessed from the symmetry of the lamination. Also, since the lamination is balanced, the A_{16}, A_{26} terms are also identically zero. Since there are no cross-ply arrangements, the D_{16} and D_{26} terms do not disappear and hence there is an elastic coupling between bending and twisting. One may also calculate the effective engineering constants of the laminate; these are found to be

Table 1. NCT304-1 Carbon/Epoxy property

Property	**Value**	**Units**
Prepreg gel temperature	300-350	ºF
Prepreg gel time	1.5	hr
Resin content	42±2	%
Tensile strength	240	ksi
Tensile modulus	18	10^6 psi
Flexural strength	245	ksi
Flexural modulus	17.6	10^6 psi
Compressive strength	128.3	ksi
Compressive modulus	17.5	10^6 psi
G_{ic} (DCB test)	2.83	(in-lb/in^2)
G_{iic} (ENF test)	7.96	(in-lb/in^2)
Poisson's ratio	0.303	Dimensionless

All results normalized to 60% Fiber Volume

* *Material Information from Newport Adhesives and Composites, Inc*

$$E_x = 56.4\,\text{GPa}, E_y = 46.1\,\text{GPa}, G_{xy} = 17.0\,\text{GPa}, \nu_{xy} = 0.324, \nu_{yx} = 0.265 \quad (3)$$

As can be determined from these engineering constants, the gradual change in the properties of the neighboring layers results in a nearly isotropic response of the laminate. To exhibit this more clearly, the variation of the engineering stiffness of the laminate as a function of the orientation with respect to the global x-direction (the direction with four layers of zeros in the middle section) is shown in Figure 3. The C_{11} and C_{22} stiffness components vary very little as a function of the orientation; it is also important to observe that the C_{16}, C_{26} stiffnesses are

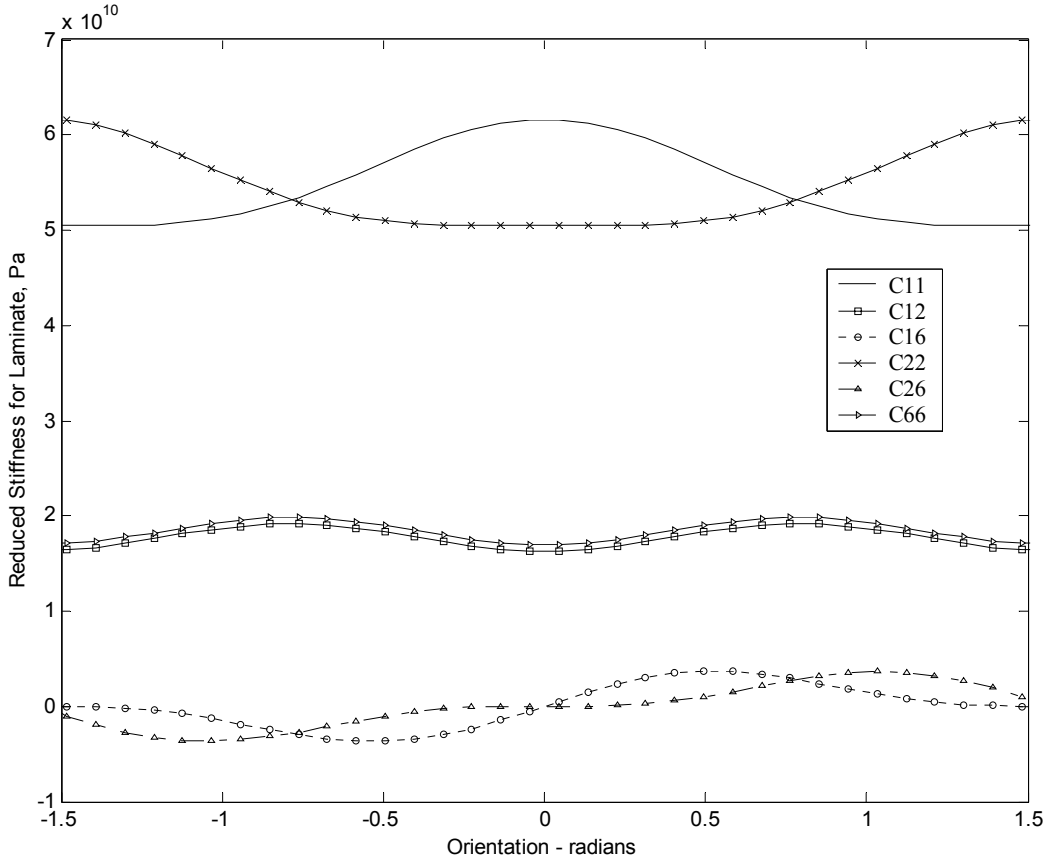

Figure 3. Reduced stiffness matrix of the laminate as a function of orientation with respect to the global x-direction.

small, suggesting that the coupling of extension to shear is small, but nonzero. If the extra layers of 0° in the middle of the plate are removed, a perfectly isotropic structure can be obtained; however, that is not the main objective of the helicoidal composite – the reduction in the interlaminar shear stresses is the primary objective.

2.2. Processing Induced Residual Stresses

The residual stresses that arise in the composite during the thermal processing of the material were evaluated with ABAQUS finite element analysis program. The model is composed of 40 different layers with fiber direction specified according to the lay-up described above. Due to the asymmetric nature of the specimens considered, the full 3-D plate model had to be employed in the simulation. In these simulations, a 12 inch by 12 inch by 0.25 inch thick square specimens were simulated. In this analysis 2500 quadrilateral elements were used per layer; each layer was provided with elastic properties corresponding to the appropriate fiber orientation. The element type C3D8; 8 noded cubic 3-D element, was chosen for this model. The analysis was performed on two specimen designs: a ± 45° specimen with 45 layers, and a helicoidal composite with the lay-up indicated in Figure 2. Transversely isotropic material properties given in Eq. (1) were prescribed for each layer, with the appropriate material direction relative to the global directions. Free edge singularities occur due to material mismatch; the extent of the boundary layer where such influence is important was considered to be small enough to not influence the development of processing induced residual stresses in the interior of the plate. Thus, coarse finite element simulations were used to provide an estimate of the cure induced residual interlaminar shear stresses in the interior of the plate.

The interlaminar stresses introduced by the decrease of temperature during the cooling cycle were analyzed by providing the coefficient of thermal expansion for the different layers, and changing of temperature from 300°F to nominal room temperature of 70°F. From the finite element analysis the interlaminar stresses from the specimen with abruptly changing ± 45° stacking orientation were found to vary abruptly across each layer and hence really unresolved in magnitude in this coarse simulation; in contrast, the helicoidal stacking sequence exhibits a gradual change in the shear stress as shown in Figure 4; it is notable that there is a continuous and gradual variation of the shear stresses. Furthermore, the magnitudes are quite small – on the order of a few hundred kPa. It is possible to further control the interlaminar stresses by prestressing selected fibers, but this was not attempted in the present study.

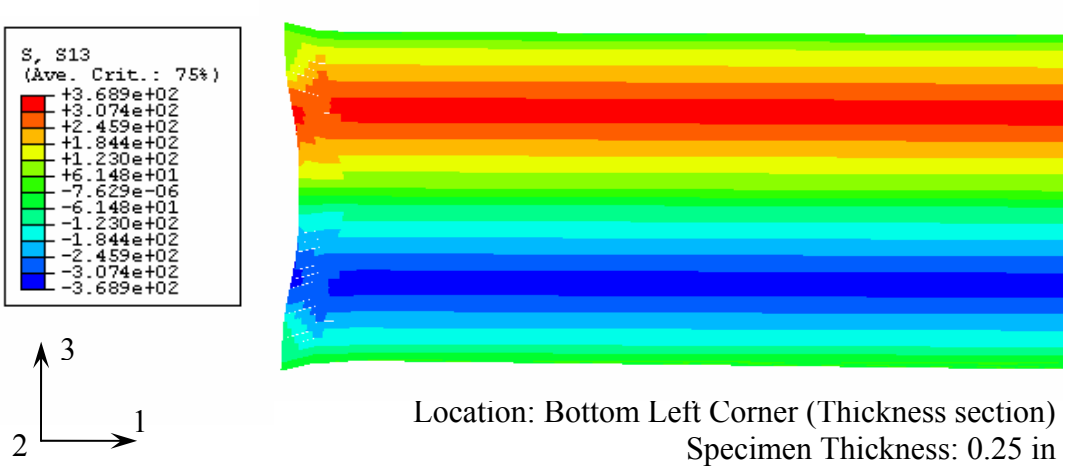

Figure 4. Residual stress distribution in the helicoidal specimen

2.3. Through-Thickness Reinforcement

For a composite material the properties of the laminate depend on the direction of individual lamina. Therefore, to obtain a high load capacity a stacking sequence of the laminate is usually generated. Delamination between composite layers due to the difference in fiber orientation is one of the most commonly observed failure modes. There have been numerous experiments and models generated to understand and predict the phenomenon of delamination in composites (the bibliography lists a selected few publications that deal with the issue; Science Citation Index indicates that there are at least 2000 references on the subject of composite AND delamination). In very early work, Chai *et al*., (1981, 1983) demonstrated that delamination was a crucial limiting factor for composites under low-speed impact. The role of interlaminar stresses and free-edge delamination in limiting the strength of composite materials has also been recognized for quite some time; the early work of Pagano (1978) set the stage for intensive investigations in this area. Based on numerous experimental investigations that revealed the mechanisms of deformation and failure in composites, micromechanics based constitutive models have been developed that capture the mechanical behavior of composite materials; a good concise summary of progress in this area can be found in the article by Dvorak (2000). This article also provides a listing of open issues in composites that require further attention. Specifically with reference to delamination, damage and failure under dynamic loading conditions, Dvorak stresses the need for further experimental and modeling research; ideas such as selective reinforcement, improved adhesion characteristics and generation of residual stresses are suggested for improving the delamination and damage resistance in composites.

Recognizing that delamination is driven by interlaminar stresses and the weak bond across the laminae, much work has been done aimed at determining the role of the lamination in dictating the damage resistance of composites under quasi-static and dynamic loading. For example, Tao and Sun (1998) performed an experiment to investigate the interlaminar fracture behavior and toughness of 0º/θ interface with θ = 30º, 45º, 60º and 90º. They found that the interlaminar toughness decreases as the off-axis θ angle increases and remains constant as θ changes from 15º to 90º. Hsiao *et al*., (1998) studied the effect of strain rate and the fiber orientation on the mechanical properties of thick carbon/epoxy composite materials. They observed that the strength and ultimate strain values increased as strain rate increased and that the specimen with transverse direction fiber has higher stiffness than the longitudinal direction. An impact analysis of laminated composite performed by Liou (1997) found that for the anisotropic laminated plate, higher stresses exist in the direction having higher stiffness and that the delamination cracks are caused by the interlaminar stresses.

Many investigators have employed through-thickness reinforcement as a way of mitigating the delamination problem. The reinforcement can be achieved by many methods such as stitching, braiding, z-fibers/z-rods, fiber waviness or adhesive strips. The experiments performed by Rugg *et al.* (1998, 2002) found that the through-thickness reinforcement by z-rods raised the critical stress for delamination significantly. For the through-thickness reinforced structure, when the delamination cracks initiate and propagate, the z-fibers or reinforcements stop the delamination cracks. The applied load must then increase to the strength limit of the reinforcement before the delamination cracks can restart propagation; the load drops until the delamination encounters the next reinforcement. This

cycle repeats until the last reinforcement is reached and total failure occurs. Therefore, the load-displacement diagram presents a stepped line instead of continuous line in an ordinary laminate, but the ultimate load is significantly increased. Geubelle and Baylor (1998) demonstrated through a cohesive zone model that localization of damage in the interlayer region can occur even before wave reflection from the plates free surface. In very recent work Baucom and Zikry (2003) and Bahei-El-Din *et al* (2003) have explored the mechanism of failure in 2D, 3D woven composites and 3D woven porous composites and utilized finite element modeling to generate constitutive modeling of the failure in these composites. They found that 3D composites had consistently higher damage tolerance than their 2D counterparts. Therefore, it appears that damage development can be controlled either through the z-reinforcement or through a 3D woven design of the reinforcement.

Modeling of delamination in order to evaluate the damage tolerance quantitatively has also been of significant interest. Many of the models have used a quasi-static approach, justifying the assumption based on the idea that the time scale of the contact is very long in comparison to the wave travel time; however, significant damage can occur during short time scales as well (see for example, Choi *et al*., 1991 and Collombet *et al*., 1996). Recently, Geubelle and Baylor (1998) used a cohesive element model to endow the delamination with a failure model that can then be used to simulate progression of damage.

For short rod reinforcements, various metallic (aluminum and titanium), or fibrous carbon rods with diameter between 0.2-0.6 mm are inserted through the thickness of the laminate (Barrett, 1996, Rugg *et al*., 1998). The area density of reinforcement is between 1-5 %. In the stitching method the prepreg laminate or fabric is inserted by a high tensile strength

yarn, which is usually made from glass, carbon or Kevlar (Rugg *et al*., 1998, 2002). In our specimens through-thickness reinforcement was provided by the stapling method which is similar to the short rod reinforcement. The staples were introduced to the laminate in the desired pattern to prevent delamination and propagation of cracks at the loaded area. The stainless steel staples depicted in Figure 5 were used. The staples had a square cross section with an area of 0.00125 in^2. The height of staple's leg is 0.24 in – sufficient to bridge across the thickness of the cured plate – and the width between two legs is 0.418 in. In order to design the pattern having reinforced area density as required to support the structure, the spacing between the staples should be considered; these were determined through three-point bend and double cantilever beam tests designed to determine the characterize the delamination toughness.

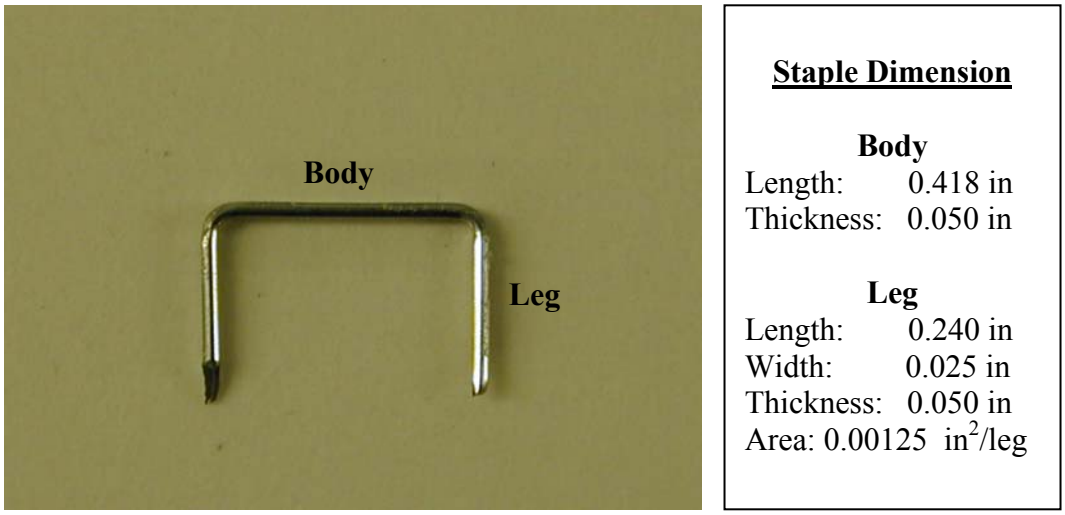

Figure 5. A close-up view of the staple-pin used for thickness reinforcement.

2.3.1. The Three Point Bending Test: Three point bending tests followed the ASTM D790, D2344 and D5934 standards and were performed on (0°)40, stapled (0°)40 and stapled (0°/90°)20 specimens. The purpose of this test was to determine the flexural stiffness of laminated composites and to compare between specimens with different stacking geometry and with and without stapling reinforcement. To prepare specimens for three-point bending test first of all the prepreg roll was cut to size 1 inch by 10 inches in the desired direction for 40 strips. Next, two kinds of specimen used in this study: one without staple-reinforcement and the second one with a staple reinforcement. For the staple-reinforced specimen, only 38 layers were stapled, keeping the last two layers for covering the top and bottom of the laminate after the complete stapling process.

By using the composite laminate calculation to evaluate the maximum interlaminar shear stress and assuming that the staples can hold the laminate without any additional supports from the matrix, the stapling reinforcement was designed to reinforce at 1% area density. The staples are chosen to be perpendicular to specimen axis because during loading if the staples are placed in the longitudinal axis, they will create some additional strength due to the stapling themselves to the specimen and cause difficulties in interpreting the experimental data. From the three-point bending loading geometry, the damage is expected to be located under the loading point. Thus the purpose and expectation from this stapling reinforcement are to increase the through-thickness strength and to stop or slow the propagation of cracks for individual stapling location.

The data from these experiments were used to determine the flexural stress, flexural strain and bending modulus of elasticity. The comparison between the specimens was

employed for analyzing the stacking geometry and stapling reinforcement effect to the specimen. The span between supports was 5 inches, corresponding to the standard requirement and 1.5 inches overhang on both sides preventing specimen from slipping off the supports when deforming. The loading pin and supports were aligned so that the axes of the cylindrical surfaces were parallel and the loading pin was midway between the supports.

A rectangular specimen strip rested on two supports and was loaded by the loading pin midway between the supports. The support span-to-depth ratio was about 20:1. When a specimen is tested in flexure as a simply supported beam with a load at the midpoint, the flexural stress can be calculated from the following:

$$\sigma_f = \frac{3PL}{2bd^2} \tag{4}$$

where σ_f is the stress in the fiber, P is load at a given point on the load-deflection curve, L is the support span, b is the width of beam, and d is the depth or thickness of beam. The flexural strain can be calculated as follows:

$$\varepsilon_f = \frac{6Dd}{L^2} \tag{5}$$

where D is the maximum deflection of the center of the beam. The bending modulus is the ratio of flexural stress to corresponding strain calculated:

$$E = \frac{L^3 m}{4bd^3} \tag{6}$$

where *m* is the slope of the initial straight-line portion of the load-deflection curve. Figure 6 shows a plot of the load-displacement results obtained from different stacking geometries, with and without through-thickness reinforcement. The unidirectional specimen had a maximum load of about 1000 lbs corresponding to deflection of 0.3 in. When the unidirectional specimen reached the maximum load, the laminate instantly broke with a corresponding rapid load drop, indicating absence of damage tolerance.

The behavior of specimen with through-thickness stapling reinforcement was different from that mentioned above. When these specimens reached the maximum load, the outer surface of the specimen broke, cracks grew and tried to propagate through the specimen and then load started to decrease. The stapling reinforcement held the specimen from sharp failure and stopped the crack propagation corresponding to each stapling location. Therefore,

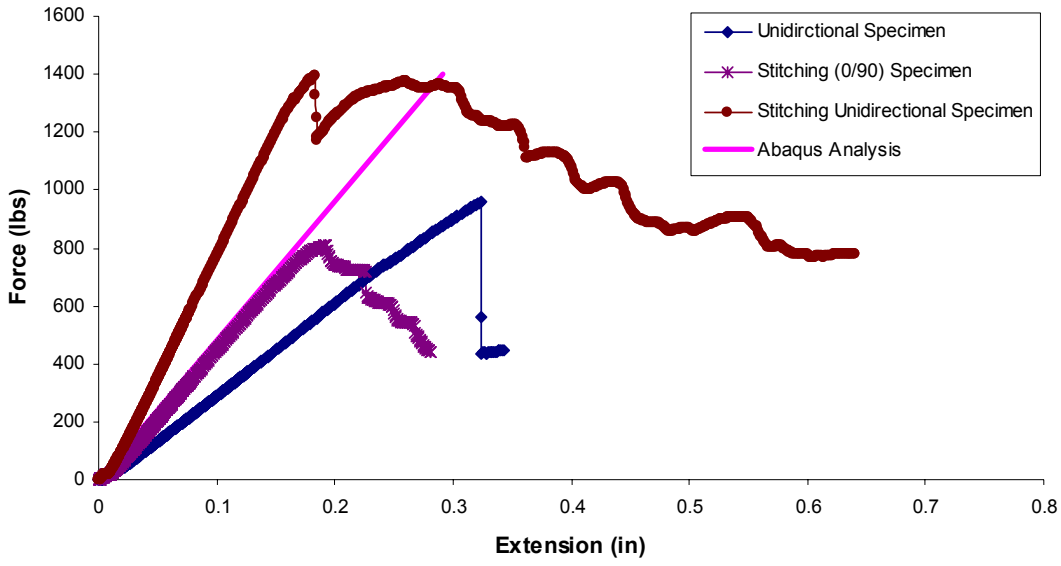

Figure 6. Load-Displacement Variation for the Three Point Bending Test

each staple increased the load until the load was higher than the staple limit. Then that staple failed and the cracks propagated to the next staple and started the new cycle until approaching the last reinforcement and the whole specimen failed.

Moreover, the energy absorption or area under the load and displacement curve of the unidirectional specimen with stapling reinforcement was 3 times higher than the specimen without staples. The comparison among the maximum load of stapled unidirectional specimen, stapled (0°/90°) specimen and the unidirectional specimen showed that the stapled unidirectional specimen had the highest load and the next highest load were without stapling unidirectional specimen and stapling (0°/90°) specimen respectively. Even though the maximum load of (0°/90°) specimen had the lowest value, the bending modulus corresponding to the slope of the graph of this specimen was still higher than the unidirectional specimen. Thus, it showed that the stapling through-thickness reinforcement of the specimen increased the load carrying capacity of the specimen and as well as the elastic bending modulus.

2.3.2. The Double Cantilever Beam Test: A double cantilever beam (DCB) test following the ASTM D5528 standard test method for mode I interlaminar fracture toughness of composite material was used to determine an appropriate choice of staple spacing. The experiment was performed on *unidirectional* staple-reinforced specimens to determine the fracture toughness and crack propagation behavior. These specimens were obtained from a single unidirectional specimen prepared from the same prepreg as all other specimens, but with staple reinforcement. The through-thickness reinforcement was expected to increase the

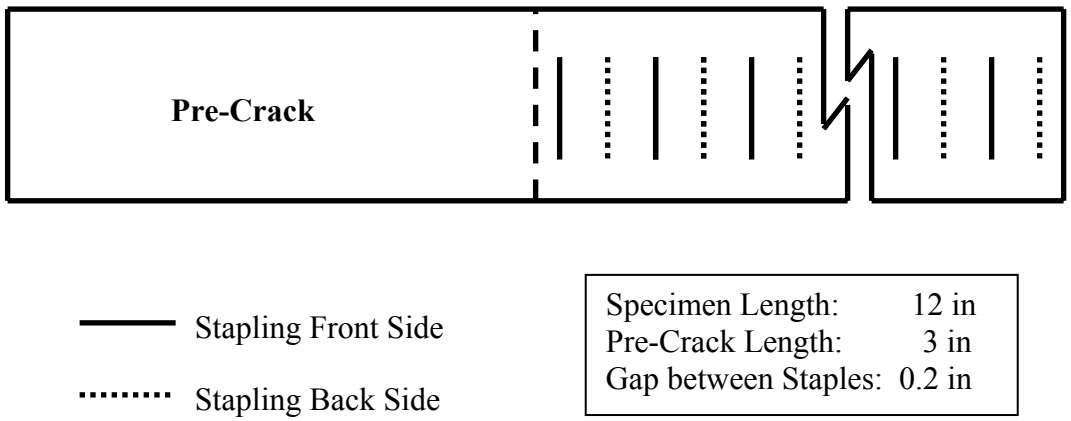

Figure 7. The reinforcement pattern for the DCB specimen (top view)

interlaminar strength and stop the propagation of the cracks corresponding to each staple location.

The reinforcement pattern shown in Figure 7 is desired for this DCB test in order to obtain a stapling area density of about 0.78% This estimate is based on the assumption that these staples can prevent crack propagation without any supports for the matrix material. The staples were located both in the front and back side at every 0.4 inch interval along the axis of the specimen. The stapling pattern was expected to increase the interlaminar strength and stop propagation of cracks corresponding to each stapling location. To manufacture this specimen with a pre-crack zone, a Teflon film is used to prevent the specimen from consolidating along the crack plane during the curing process. Teflon film was chosen for its small thickness, high temperature resistance, and poor adhesion to the prepreg so that is easily removed from the cured specimen.

The staple locations were marked on the edge of the specimen by a marker pen or white color dye for reference to determine the location of the crack tip. Hydraulic grips were attached on the bottom and top crossheads of the machine. The bottom and top grips were aligned to prevent any twisting during loading by using a solid bar for adjusting the position. Aluminum end tabs were attached to the specimen and connected to the hydraulic grips. During the experiment a high resolution video camera was used to record the specimen profile. Image processing software was used to determine the crack length and opening displacement. A picture of the specimen under load as captured by the video camera is shown in Figure 8.

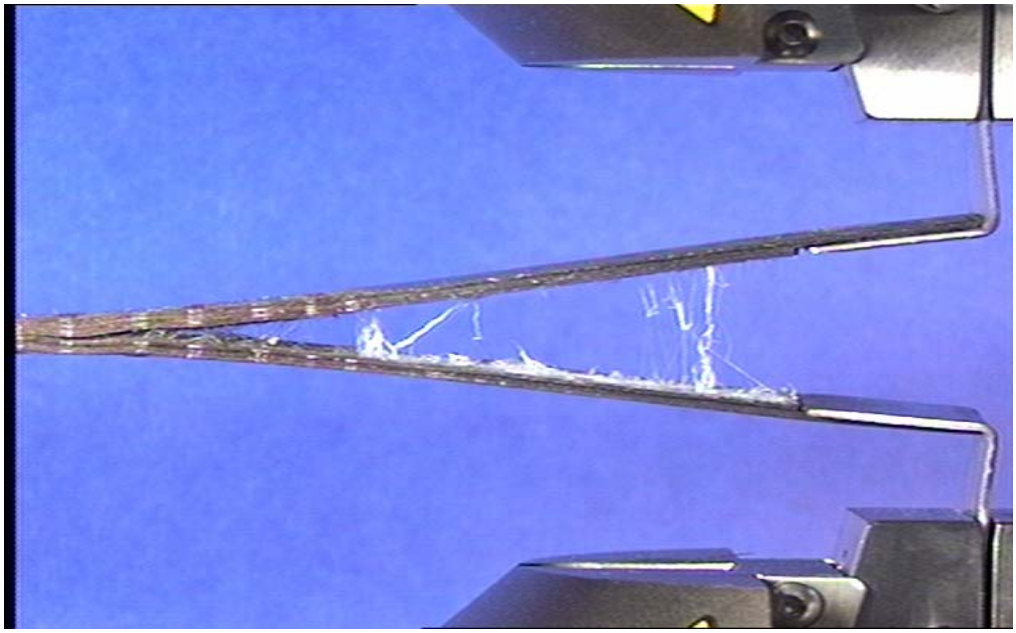

Figure 8. Double cantilever beam specimen test for the determination of the interlaminar fracture toughness.

The ends of the DCB specimen were loaded by controlling the crosshead movement, while the load and delamination length were recorded by the external computer. As recommend by ASTM standard the crosshead speed operated at 0.1 in/min. The interlaminar fracture toughness G_I was determined from a simple analysis as follows:

$$G_I = \frac{3P\delta}{2ba} \tag{7}$$

where, P is the load at crack initiation, δ is the load-point displacement, b is the width of beam and a is the crack length. Figure 9 shows a plot of the load and crack opening displacement obtained from a through-thickness staple-reinforced specimen. The graph reveals that the load increases corresponding to the increasing of displacement until the load

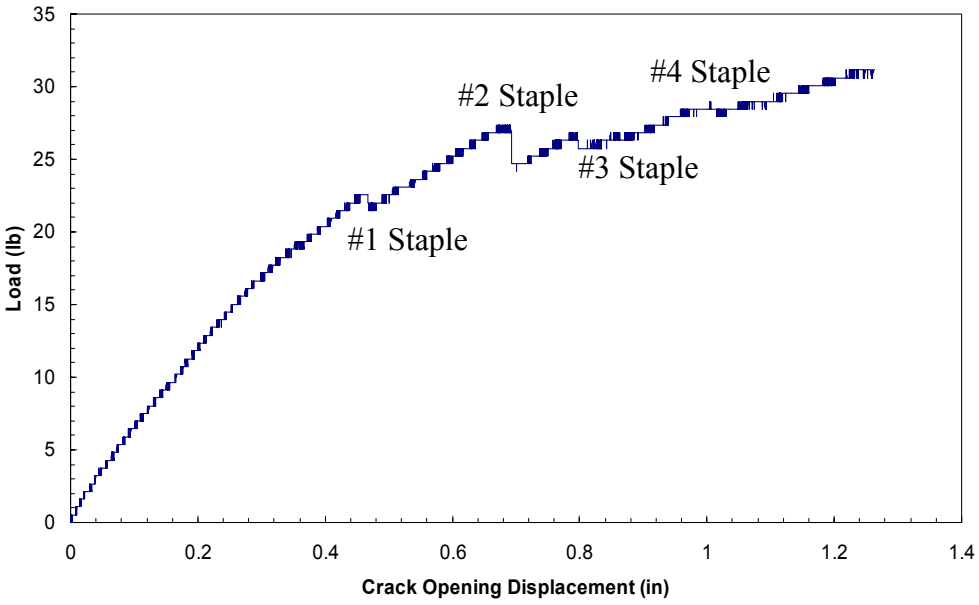

Figure 9. Variation of the load with crack opening displacement for the DCB test.

reaches a value when the crack starts to propagate; corresponding to this there is a drop in the load. However, the crack is unable to grow through the reinforcing staple and arrests. The load has to increase further before breaking through the next staple. This behavior was observed at every staple; the break point of each staple is identified in the figure. The interlaminar fracture toughness was determined from Eq. (7) and the test data. A plot of interlaminar toughness normalized by the matrix fracture toughness K_{IC} = 1.19 ksi-in$^{1/2}$ and crack growth distance is shown in Figure 10. In this graph the toughness was calculated both at the onset of crack initiation and at the point of arrest using the peak and minimum loads at each crack popping event. It is apparent that there is a toughening trend in the stapled composite with the toughness increasing by more than a factor of two as more staples bridge across the crack that had propagated through the matrix layer. This kind of bridging is the main reason that the stapled composites can exhibit stable crack growth. The reinforcement used occupied only 1.35% of the total cross section; clearly there is the possibility to increase the toughness even further through an optimization technique to determine the best possible staple property and the best possible geometrical arrangement.

Based on the DCB results, the reinforcement pattern was designed to provide a stapling area density of about 1.35% to support the delamination force calculated from plate bending theory. The staples on the front and back side of the specimen were located on concentric circles starting from the smallest circle at the center of the plate under the loading area. The distance between the stapling circles is 0.25 inch alternatively between the front and back side. The position of staple is chosen to be perpendicular to the radius of specimen for preventing any contributions to the in-plane strength that does not come from the through-

thickness reinforcement. The stapling pattern is expected to arrest the propagation of cracks and increase the interlaminar strength for individual stapling location. The laminate stacking procedures were slightly different for the stapled specimen; only 38 laminae were placed before the stapling process and the last 2 laminae were used to cover each side of the laminates. A view of the specimen after completing the stapling reinforcement is presented in Figure 11.

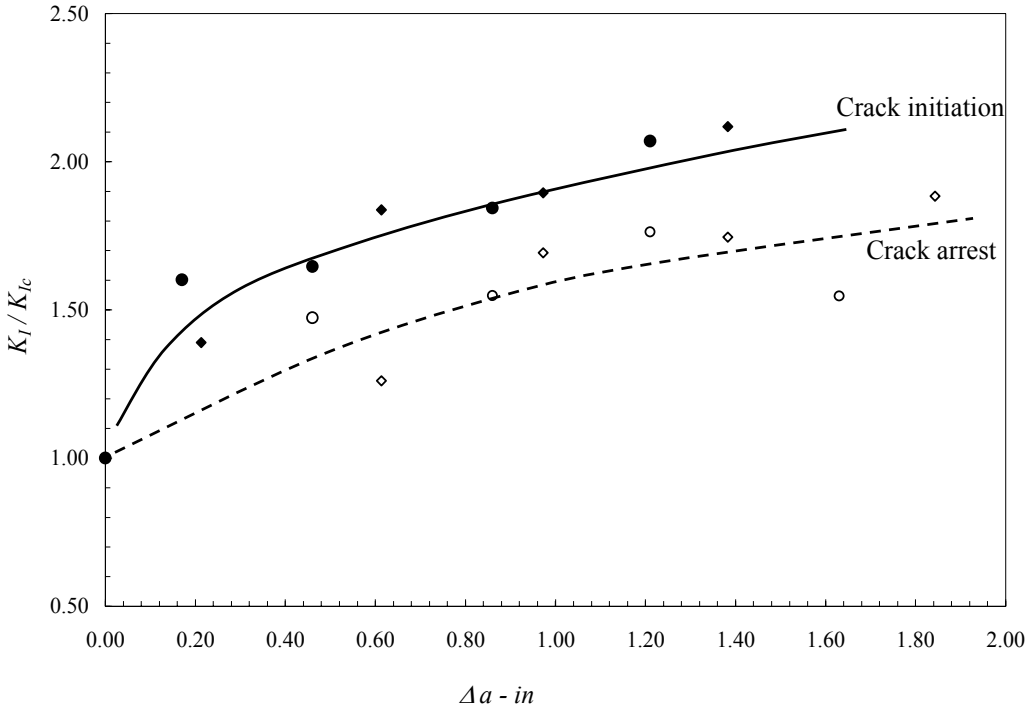

Figure 10. Variation of the fracture toughness K_I/K_{IC} and crack length (staple-reinforced specimen).

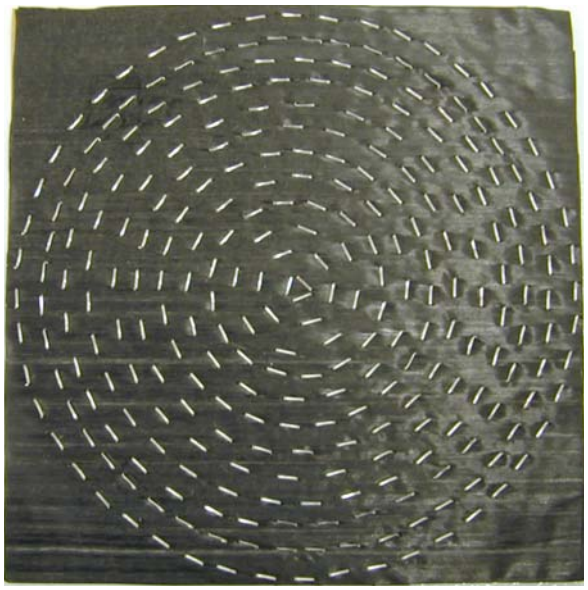

Figure 11. Staple-reinforced circular plate prior to curing

3. FABRICATION OF HELICOIDAL COMPOSITES

A standard hand lay-up and vacuum bagging process was used for manufacturing composites. The prepreg of the composite material studied in this research was manufactured by Newport Adhesives and Composites, Inc. The nominal properties of the fiber and matrix are shown in Table 1. The prepreg carbon-fiber epoxy NCT304-1 supplied in the form 36 inches wide continuous roll were cut to the desired size, (12 inches long by 12 inches wide), in a large shear cutter. For the helicoidal composite the stacking sequence of the specimen required 40 layers cut in the different orientations according to the lay-up in Figure 2. Therefore by using a cutting pattern corresponding to individual directions, the prepreg were cut according to the desired orientations. The next step after obtaining multidirectional cut laminas was stacking the specimen in the correct sequence. Good alignment (deviation ±2° for the hand lay-up process) of each layer was very important because greater misalignment between the layers would change the properties of the laminate significantly. While the layers were stacked to form the laminate, trapped air bubbles were removed by rubbing the top layer with the interleaving paper simultaneously.

After obtaining the complete stacked laminate the stack was placed in a vacuum bag. The purpose of vacuum bagging is to remove air pockets and voids that could form in the composite during curing process. The stacked laminate was placed between two one-inch thick aluminum plates, and the thermocouples used to monitor the temperature distribution around the specimen plate were attached. Next, the vacuum bag was sealed by the sealant tape. Finally, the vacuum bagging assembly was inspected by connecting the thermocouples to temperature channels in the autoclave and attaching vacuum connector to the vacuum hose

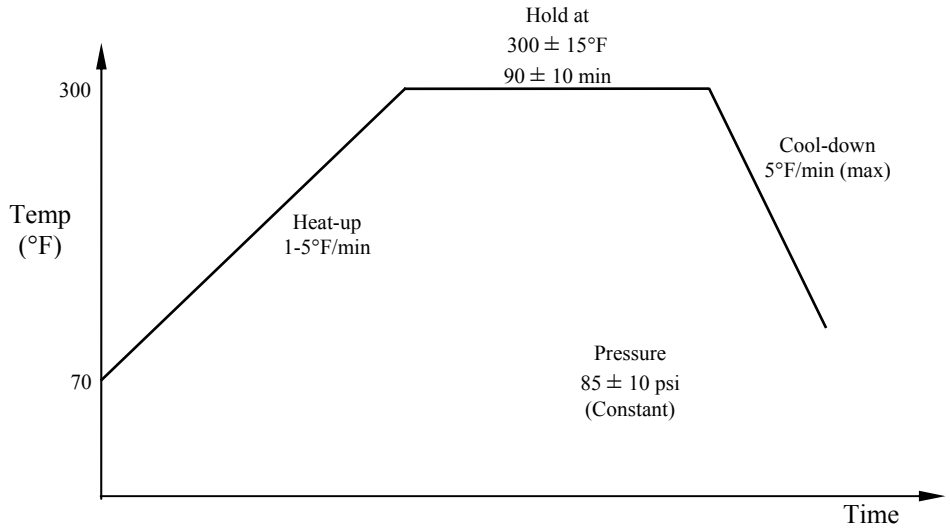

Figure 12. Temperature and pressure cycle used for curing the helicoidal composite

for inspecting the sealing system. For curing the composite, the laminate plate was placed in an autoclave and subjected to the temperature and pressure history shown in Figure 12. The temperature and pressure cycle used in the autoclave for curing the specimen is comprised of three steps: the heat-up, curing and cool-down. According to the manufacturer's material data sheet the temperature and pressure cycle in the autoclave should be as shown in Figure 12.

For the consolidation process, the vacuum bagged assembly was located inside the autoclave chamber to heat and pressurize along the curing profile. In order to obtain good quality laminates the temperature and pressure distribution should be controlled precisely. Some preliminary tests were run to obtain the distribution of temperature gradients inside the chamber in order to determine the areas with the most uniform temperature distribution in the chamber. A few tests were also set up to monitor the thermal gradient through the thickness of the plate; in these tests six thermocouples were placed at the center of different locations

to display through the thickness temperature of the quarter inch thick composite specimen as shown in Figure 13. The pressure in the autoclave was controlled by adjusting the pressure valve to set-up the pressure corresponding to the manufacturer's recommended consolidating pressure of 85 psi. For curing laminate the temperature was increased at about 1-5°F/min until approach to the recommended curing temperature of the epoxy matrix (around 300-350°F, see Table 1) and maintained at the constant level for 1.5 hours. After the plate was cured, the cooling process was performed simply by turning off the power to the autoclave; the cooling rate was quite low and it took around 6-7 hours before the temperature decreased below 70°F.

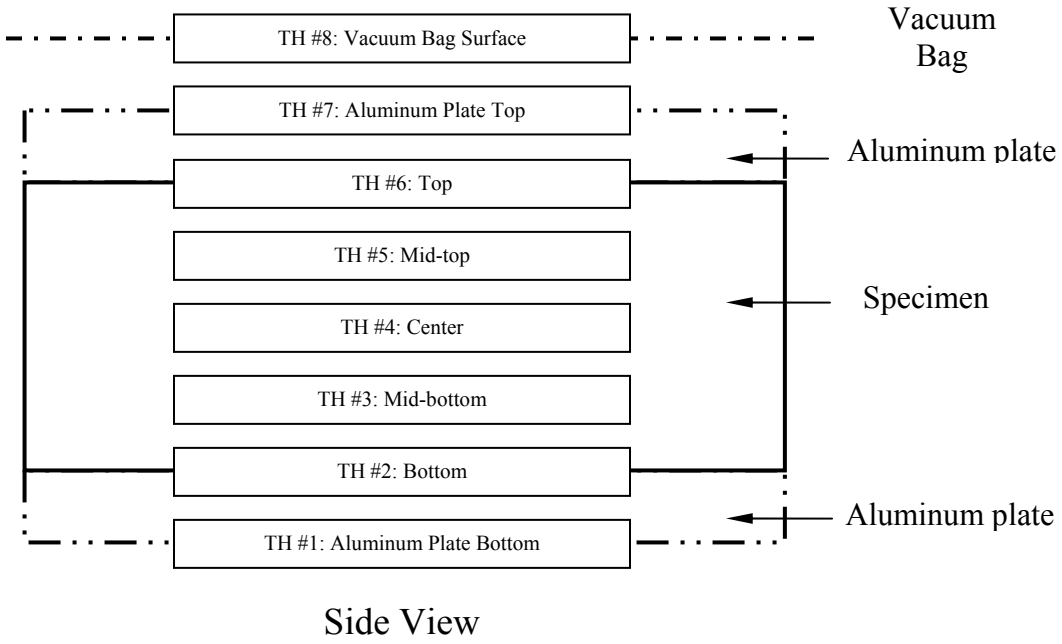

Figure 13. Location of the thermocouples for evaluation of the through-thickness temperature distribution.

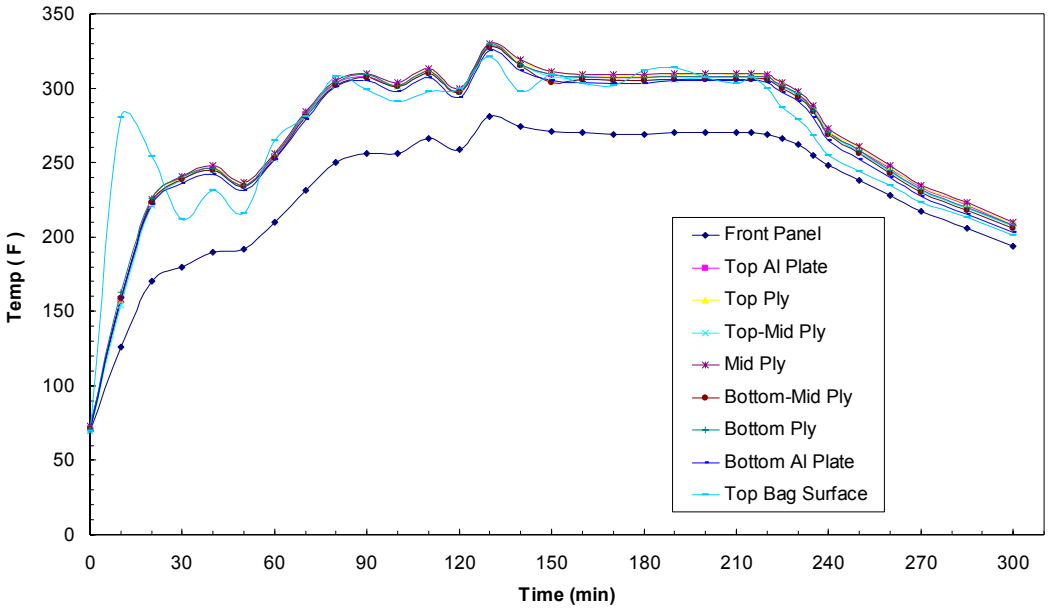

Figure 14. Through-thickness temperature distribution in the specimen during curing.

As shown in the graph in Figure 14 the temperatures displayed by thermocouples inside the specimen and between specimen and tool plates were quite uniform. Even though there were some deviations of the specimen temperature from the set-point and the outside surface of vacuum bag during the heating cycle, the overall results were satisfactory. Thus these results provide assurance that the specimen should have an even temperature distribution during curing process. During fabrication, the temperature distribution was monitored with eight thermocouples placed in specific locations around the tool plates and the vacuum bag. After removing the cured laminate from the autoclave, an ultrasonic C-Scan was used to inspect the quality of the specimen.

The process described here was used to fabricate 12 in long 1 in wide specimens for the DCB tests and the three-point-bend tests described in Sections 2.3.1 and 2.3.2, as well as the

12 in by 12 in circular plate specimens without and with staple reinforcements for use in the plate bending and impact tests. Specimens for uniaxial tension tests were obtained by machining the 12 in x 12 in plates. The uniaxial and ±45° specimens used for comparison were graphite epoxy specimens that were available in our laboratory from previous studies; their true composition was unknown and hence we used the uniaxial tests as the baseline properties for these specimens.

4. MECHANICAL CHARACTERIZATION OF THE HELICOIDAL COMPOSITE

Three basic categories of tests were performed in order to determine the mechanical characteristics of the helicoidal composite. First, the tension test was used to determine the basic properties of specimen for the different stacking geometries; the failure mechanisms for the helicoidal specimen were compared with those of a unidirectional and ±45° specimen. Second, the response of a circular laminated plate specimen with the helicoidal architecture with a clamped boundary condition was evaluated and compared with specimens of different stacking geometry and specimen with and without stapling reinforcement. Finally, the impact response of the helicoidal composite was evaluated by impacting the laminate with a high velocity striker and then observing the specimen after impact; the failure resistance behavior of the different specimens was compared. Whenever possible, standard test methods and machines were employed.

4.1. Uniaxial Tension Test

The tension test was performed following the ASTM D3039 standard test method. This test was performed on the unidirectional, ±45° cross-ply and helicoidal specimens. The purpose of this test is to understand the deformation and failure mechanisms under tension load of helicoidal specimen compared with the conventional unidirectional and ±45° stacking geometries. The 12 in by 12 in laminates that were fabricated were sectioned in a milling machine to obtain 12 in by 0.75 in specimens suitable for the uniaxial tension tests. Before starting the experiment the quality of the specimen was checked and the dimensions were recorded. The system alignment was also evaluated before starting test. Material testing was

performed in an Instron Model 4482 Universal Testing System. The specimens were attached to a hydraulically operated wedge gripping system. In this test displacement control was used by setting crosshead speed to 0.02 in/min. The test stopped when the load dropped more than 5% or when the specimen broke. The nominal strain was calculated based on the crosshead displacement and the distance between the grips; the strain in the specimen is slightly smaller due to compliance in the load train, but this was ignored since our interest is in the comparison of the stiffness for different fiber architecture.

Figure 15 shows a plot of the stress-strain response for the unidirectional, ±45° and helicoidal specimens. For the unidirectional specimen the stress-strain response was nearly linear until abrupt and total failure. This is due to the fact that the fiber property dominates the overall specimen characteristics. The modulus of elasticity was approximately 8 million psi and the maximum stress before failure was 91 ksi corresponding to a strain of about 1.4%. A repeat test shows some variability, possibly due to gripping effects. Since the specimens were quite thick – about 0.25 in – we did not use end tabs to reduce the stress concentration; however, since the failure occurred at the grips we suspect that the measured strength is not representative of the material.

The ±45° cross-ply specimen exhibited a non-linear behavior with significant inelastic strain; the nonlinearity is due to the scissor like action of the fibers in both directions during loading. The response of this specimen was dominated by the matrix which has a low modulus; the stiffness of the specimen is correspondingly lower. The matrix dominance also results in the high strain observed prior to failure. The stress exhibits a plateau at about 10 ksi

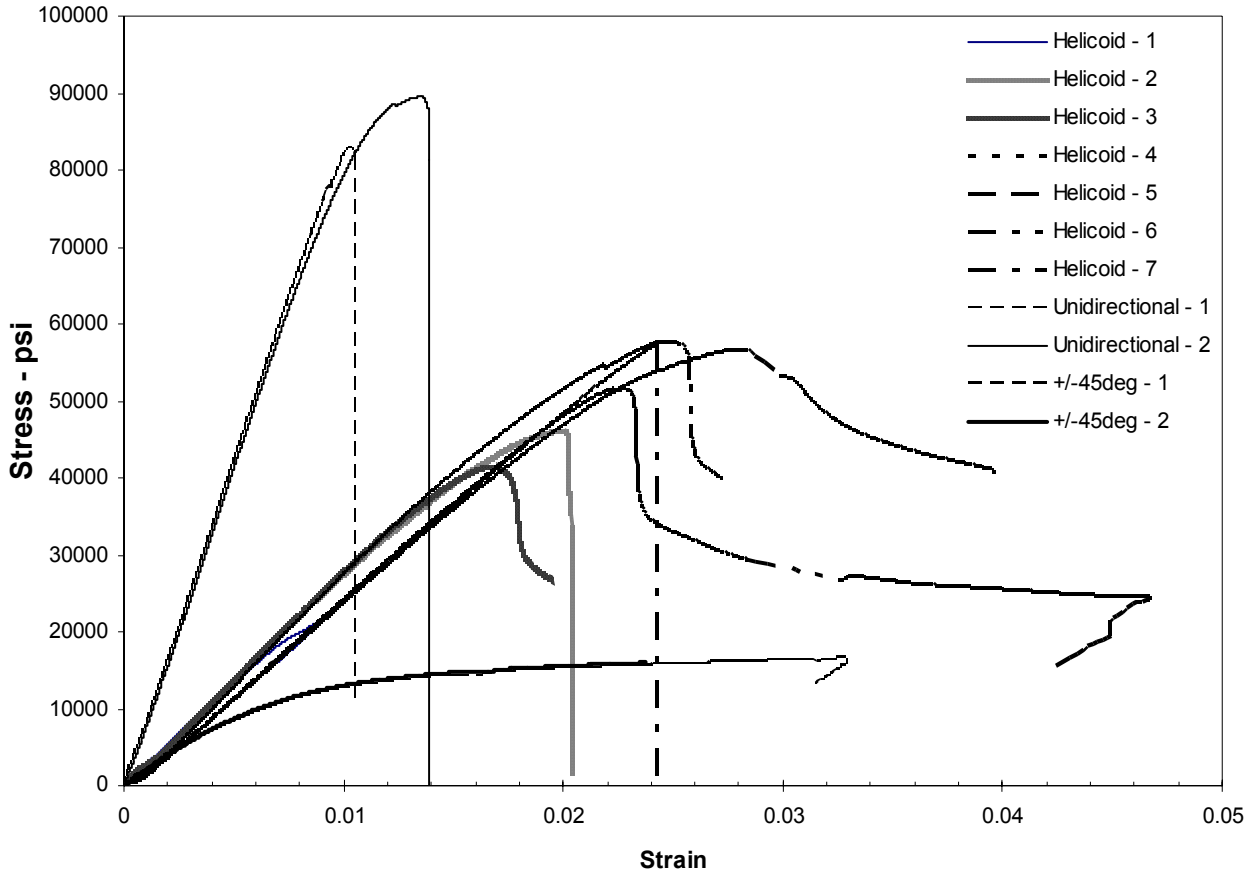

Figure 15. Results of uniaxial tension tests on uniaxial, ±45° and helicoidal specimens.

and beyond this, a nearly perfect plastic behavior is observed up to the failure strain level of about 3%.

For the helicoidal specimen the stress-strain curve showed an almost linear relationship until fairly high nominal strain of about 2%; this response is located somewhere between the unidirectional and ±45° specimens. Results from seven specimens are plotted in Figure 15 to indicate the repeatability of the response. The strength variability is primarily due to edge effects – delamination begins at the machined edges and there is a statistical variation in these flaws. It should be recognized that only six of the 40 layers were in the direction of the

load; hence the reduction in the stiffness to approximately 2.7 million psi and a reduction in the strength to ~60 ksi. When compared to the cross-ply composite, the helicoidal composite exhibits significantly higher stiffness, strength and damage tolerance. The failure mechanisms in the helicoidal composite are examined next.

4.2. Failure Mechanisms in the Helicoidal Composite under Uniaxial Tension

Examination of the failure patterns of helicoidal specimen is quite illuminating in identifying the underlying reasons for its significant damage tolerance. An example of a helicoidal specimen broken under uniaxial tension is shown in Figure 16. A complex pattern of matrix cracks and fiber breaks is generated progressively. Matrix cracks in conventional composites under uniaxial tension typically form transverse to the loading directions in the 90° layers; these matrix cracks subsequently cause fiber breaks. In the helicoidal composites, matrix cracks can form transverse to the loading direction only in two of the layers – the 90° layers. In all other layers, matrix cracks form at different angles according to the fiber architecture, but are all less than 90°. This is clearly observed in Figure 16 where arrows are drawn to indicate the planes and directions of matrix cracking in the different layers. Furthermore, the locus of tangent lines to the surface of the matrix cracks in each layer forms a helix mimicking the fiber orientation in each layer.

A longitudinal section of the broken specimen, cut along the line AA in Figure 16 is shown in Figure 17. The different layers are identifiable by the presence of a matrix rich layer in between that shows up bright in the micrographs. The distance between these bright stripes is about 178 μm, the layer thickness. The loading direction is in the vertical direction in these pictures. Transverse cracks at an angle to the main loading direction are clearly visible in these micrographs. Micrograph (a) is close to the midplane of the specimen, where the fiber orientation is along the 0° direction. The cracks are now nearly vertically aligned; these are really delaminations between the fiber and matrix rather than matrix cracks. Micrographs (b) and (c) are from regions that are from layers that are close to the 90° layers

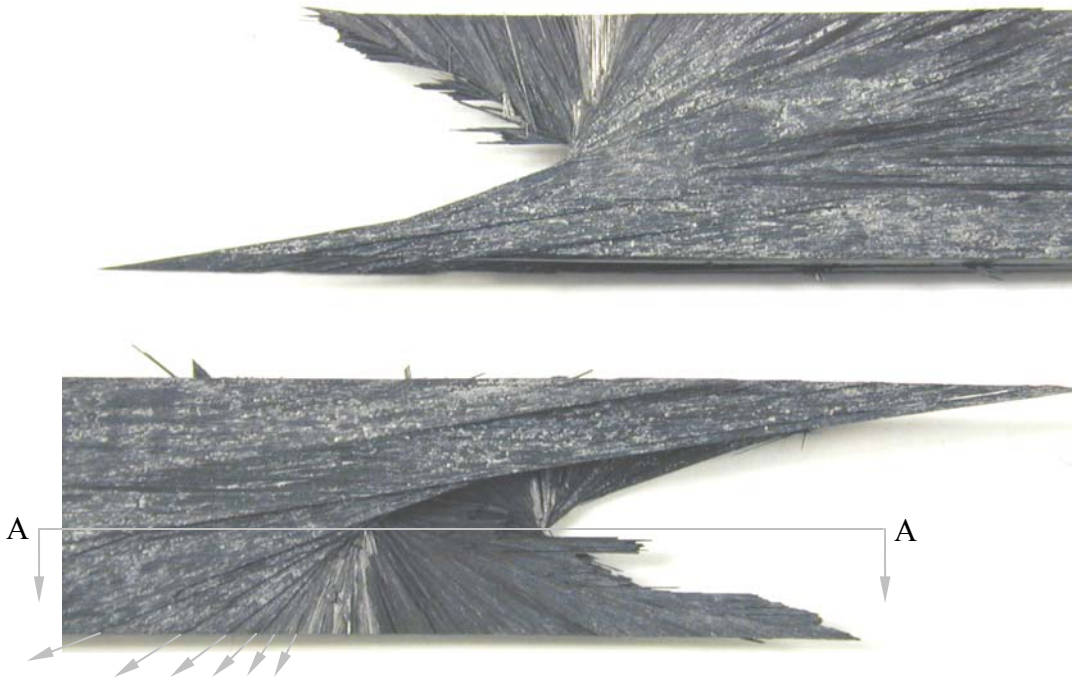

Figure 16. The failure pattern of helicoidal composite specimen under uniaxial tension. The arrows drawn suggest that in successive planes, the fracture propagated along different planes and directions.

on either side of the plane of symmetry. The progressive increase in the orientation of the matrix cracks is evident in these images. However, in these layers, the resolved normal stress perpendicular to the fiber direction is smaller and hence a larger global load is required to initiate the cracks. The linking of these matrix cracks from the different layers occurs through matrix fiber debonding. The distributed and progressive nature of failure results in a significant increase in the damage tolerance of the helicoidal composite architecture.

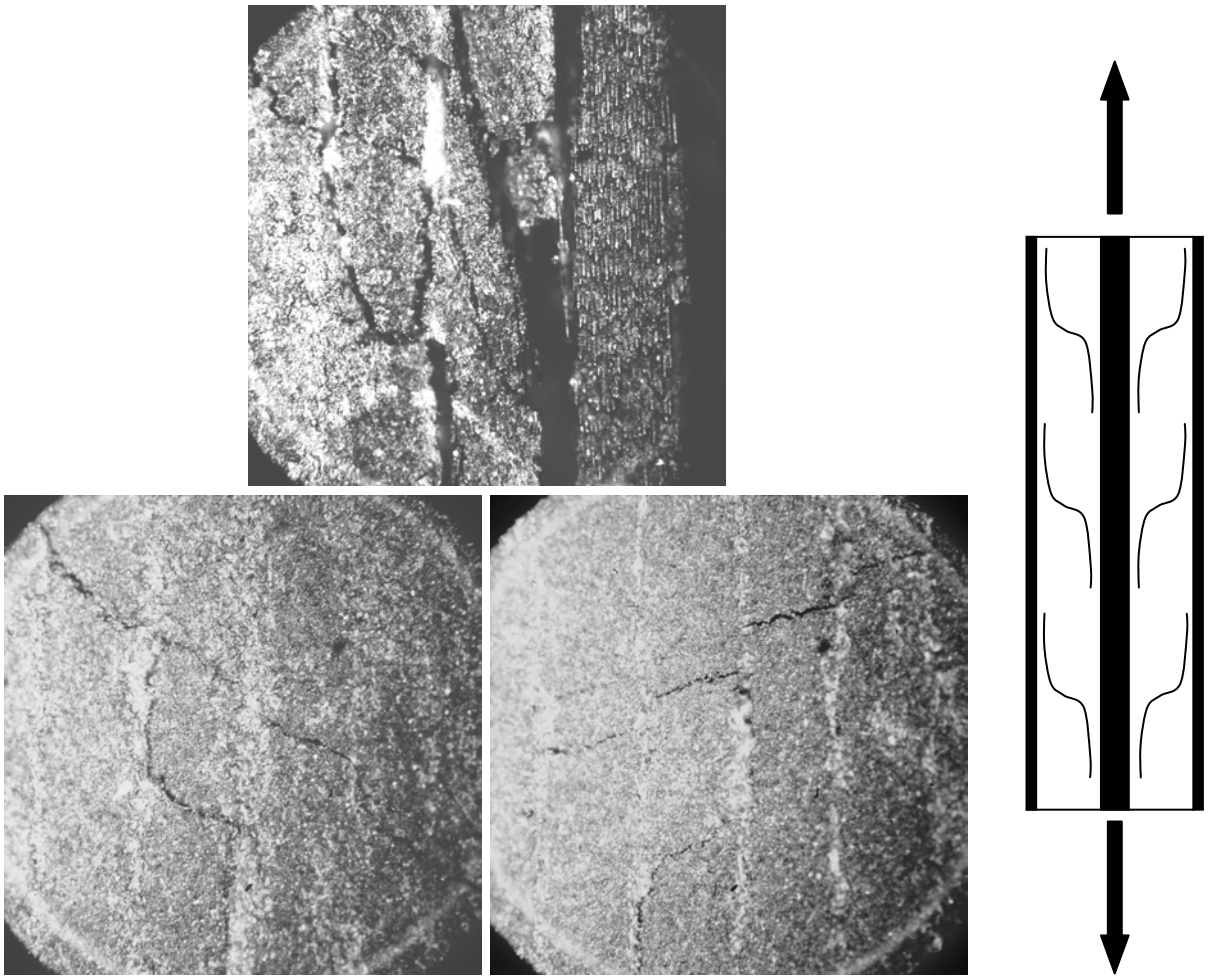

Figure 17. The failure mechanism of helicoidal composite specimen under uniaxial tension. Multiple matrix cracks in different layers are shown. A schematic diagram of the overall development of matrix cracks is shown to the right of the photographs.

While the helicoidal composite appears to possess superior properties in comparison to the ±45° cross-ply specimen, its strength under uniaxial tension is still low in comparison to the unidirectional specimen. This is simply due to the fact that even in the helicoidal composite specimen, cracks begin to grow from near free surfaces as a result of interlaminar stresses. Considering that the primary failure mechanism of matrix cracking still remains, only delayed by the architecture, through-thickness reinforcement or generation of residual stresses through processing should be considered.

4.3. Plate Bending Test

In order to obtain the true material properties of the helicoidal specimens, they must be evaluated without introducing free surfaces where the interlaminar stresses and edge delamination control the strength. The "true" strength of the helicoidal composite was evaluated by testing the entire cured plate as one circular plate subjected to a transverse point load at the center of the specimen. A fully constrained circular boundary condition was imposed by clamping the composite specimen between two one inch thick aluminum plates. For loading the specimen, a high strength sperical ball of diameter 0.5 in was employed, creating point load at the center of laminated plate. The crosshead was set to move at 0.1 in/min to generate a static load on the specimen. A photograph of the experimental set up with the specimen is shown in Figure 18. The plate bending test on the circular plate was performed on four kinds of specimens – a unidirectional specimen, ±45° specimen, helicoidal specimen and staple-reinforced helicoidal specimen – in order to compare the properties of the specimen as a function of the stacking geometry and through-thickness reinforcement.

Moreover, the finite element analysis software ABAQUS was used to perform an analysis of this test for the helicoidal geometry, without reinforcement. Post-processing was employed to determine the stress distribution in the specimen after loading and to compare the results with the experimental data and the theory of plates. The model is composed of 40 different fiber layers with layer properties depending on the stacking direction of individual layer. Because the plate was not symmetric for the helicoidal laminate, the full 3-D plate model had to be simulated. The model was composed of 2500 quadrilateral elements per each layer and each layer had elastic properties corresponding to the appropriate fiber orientation for the specimen. The element type C3D8; 8 noded cubic 3-D element, was selected. The boundary condition corresponding to the loading geometry was fixed along a circular ring in the specimen. The load at the center of the model was prescribed in the simulation.

Figure 18. Plate bending test. The composite specimen is clamped between two thick aluminum plates and bolted down. A steel ball attached to a ram is used to apply the load at the center of the plate.

Figure 19 shows a plot of the load and displacement obtained from testing the different specimens with and without through-thickness reinforcement. In order to facilitate comparison of the results from the different specimens with differing thicknesses, the load P is normalized by t^3 and the deflection w is normalized by t. Such normalization is motivated by the expression for deflection for an isotropic material; the radial variation of the deflection of the plate under loading point is given by (Timoshenko, 1940):

$$w(r) = \frac{Pa^2}{16\pi D}\left[\frac{2r^2}{a^2}\ln\frac{r}{a} + \left(1 - \frac{r^2}{a^2}\right)\right] \tag{8}$$

where, w is the deflection of the plate, P is the load, a is the radius of the plate, D is the flexural rigidity, $D = \frac{Et^3}{12(1-\nu^2)}$, E is the modulus of elasticity, t is the plate thickness, and ν is the Poisson's ratio. Since the helicoidal composite is very nearly isotropic, the above expression should provide a meaningful prediction of the deflection. However, for the actual composite architecture, the finite element analysis described above was also used for comparison with the experimental data. Specific values of the maximum load and deflection are shown in Table 2. A number of important observations can be made from the results displayed in Figure 19 and Table 2.

- The nonlinearity observed in the initial stages of loading in all of the specimens is due to the indentation of the spherical loading ball into the surface of the composite specimen; this is reminiscent of indentation experiments.

- The unidirectional specimen exhibits the weakest response. At the peak point, the maximum load is 703 lbs corresponding to a load-point displacement of 0.187 in, the laminate instantly broke to two parts as shown in Figure 20a; the load dropped abruptly to zero and total specimen failure occurred. This is consistent with a matrix failure mode; once the normal stress at the outer layer under the loading point reached the maximum allowable stress in the matrix, the matrix cracked. However, since there are no barriers to the growth of these cracks, once initiated, they grew over the entire thickness and snapped the plate into two pieces.
- For the ±45° specimen, the maximum load before onset of failure was 2520 lbs at 0.274 inch of load-point displacement. When the specimen reached the maximum load, a crack popping sound was heard and the load dropped only slightly; unlike the uniaxial specimen, matrix cracks do not have an unhindered path all across the plate thickness. The matrix cracks developed gradually in the different cross-plies resulting in an accumulation of damage at nearly constant load as the crosshead displacement was increased. Each load drop in this stage could be attributed to cracking of a particular layer. After several layers were broken, the damage accumulation became unstable (at a deflection of 0.364 in) and the load dropped abruptly to about half the maximum value as the cracks propagated. Figures 20b and 20c show images of the top and bottom sides of the specimen at failure. On the top side of the specimen two short crack segments aligned along the fiber directions of ±45° can be seen. On the bottom side, the tensile stress due to bending caused one of the cracks aligned along the fiber direction to spread completely across the specimen diameter, causing total failure of the specimen. The large residual

load carrying capacity observed in Figure 19 was merely the result of loading two semi-circular plates with clamped boundaries.

- Next, the specimen with helicoidal stacking had the highest maximum load among the configurations considered. The maximum load was equal to 5100 lbs corresponding to a load point displacement of 0.55 inch. Remarkably, the response was completely linear and elastic over the entire range, except for the irreversibility associated with the indentation at the loading point. When the load approached the maximum value, matrix and delamination cracks initiated and propagated to the ends of the specimen and the specimen failed completely. Once again, the residual load carrying capacity is from the clamped semi-circular plate effect. Figures 20d and 20e show the helicoidal specimen after failure. On the top side, localized damage near the indentation point is seen. On the bottom side, a long crack along the 0° fiber direction grew along the entire diameter of the plate. A crosssectional view indicated that delamination had occurred as well.
- The maximum load for the helicoidal composite when normalized for differences in the plate thickness is about three times that of the ±45° specimen and six times that of the unidirectional composite specimen. This result suggests that for the same material investment, the helicoidal architecture is capable of increasing the maximum load carrying capacity. However, the brittle nature of the failure suggests that once cracks are initiated, there are no barriers to their growth; hence there is no damage tolerance. This is addressed through the reinforcements in the thickness direction, generated by the staples discussed in Section 2.3.

- The behavior of the helicoidal specimen with through-thickness staple reinforcement was very similar to the one without reinforcement in the linear elastic region. The stiffness and the maximum load capacity of the specimen were not influenced by the reinforcement as expected – because the areal density of the staples was only about 1.3% – but the failure pattern was altered quite significantly, exactly as intended. When the helicoidal specimen with through-thickness reinforcement reached the maximum load, the cracks started under the load point at the center of the specimen; corresponding to this there was a sharp load drop. However, the stapling reinforcement arrested the growth of the delamination crack at the location of the first staple. Therefore, the load drop was only about 20% of the maximum load. In contrast, in the unreinforced specimen, at first crack initiation, the load dropped almost by 80%. Subsequently, under continued load point displacement, the crack ran through each staple, starting and stop at each staple until the shear stress at that staple exceeded the limit of the pin. This process continued and the load-displacement diagram in Figure 19 indicates this gradual reduction in the load carrying capacity. The specimen was unloaded after some amount of damage accumulation in order to demonstrate the residual load carrying capacity Thus, the through thickness reinforcement of the helicoidal composite is seen to endow the specimen with significant damage tolerance.
- Figures 20f and 20g show the top and bottom sides of the staple-reinforced specimen after failure. Particularly noteworthy is the fact that on the top side of the specimen crack growth was not observed at all. The damage on the bottom side is simply a bulge that occurred as a result of the spherical indentation ball punching through the specimen. At

this point, there is very little damage away from the indentation point and the specimen still retained significant load carrying capacity.

In this study, we made no attempt to optimize the position of the staples; this remains to be examined. However, there has been a clear demonstration of the increased load carrying capacity of the helicoidal composite architecture as well as the graceful failure characteristics of the through thickness reinforcement for this design. We now address the impact response of the helicoidal composite material.

Table 2. Maximum load and deflection in the different specimens

	P_{max} *lb*	w_{max} *in*	P/t^3 *lb/in*^{3}	*w/t* -	*t* *in*
Uniaxial	703	0.187	57808	0.81	0.23
±45 - begin damage	2520	0.274	140831	1.01	0.27
±45 - unstable	2670	0.364	140249	1.34	0.27
Helicoid	5009	0.519	362379	2.16	0.24
Helicoid w/staple	5006	0.526	365282	2.2	0.24

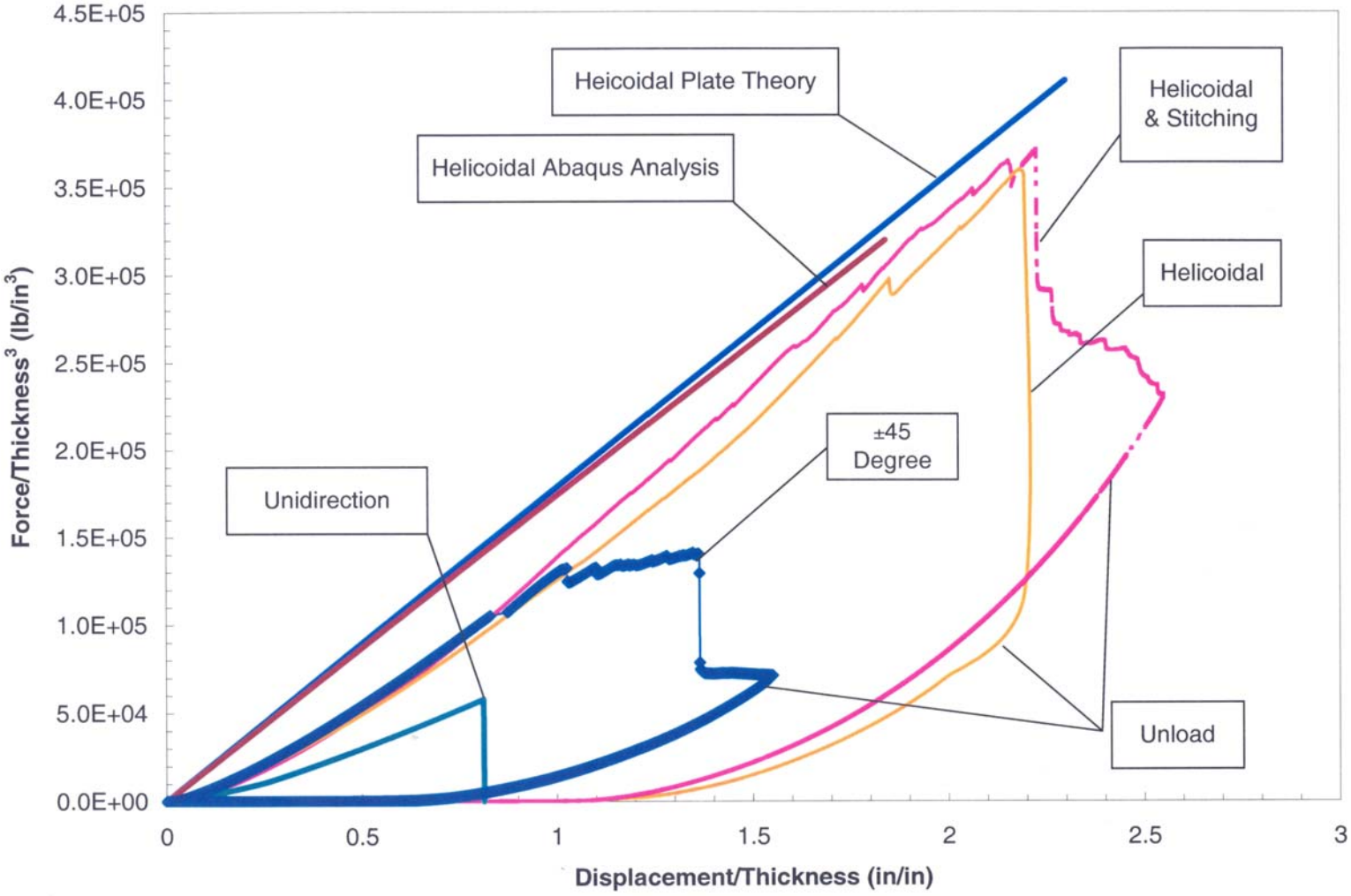

Figure 19. Load and Displacement Relationship for the Circular Plate Bending Test

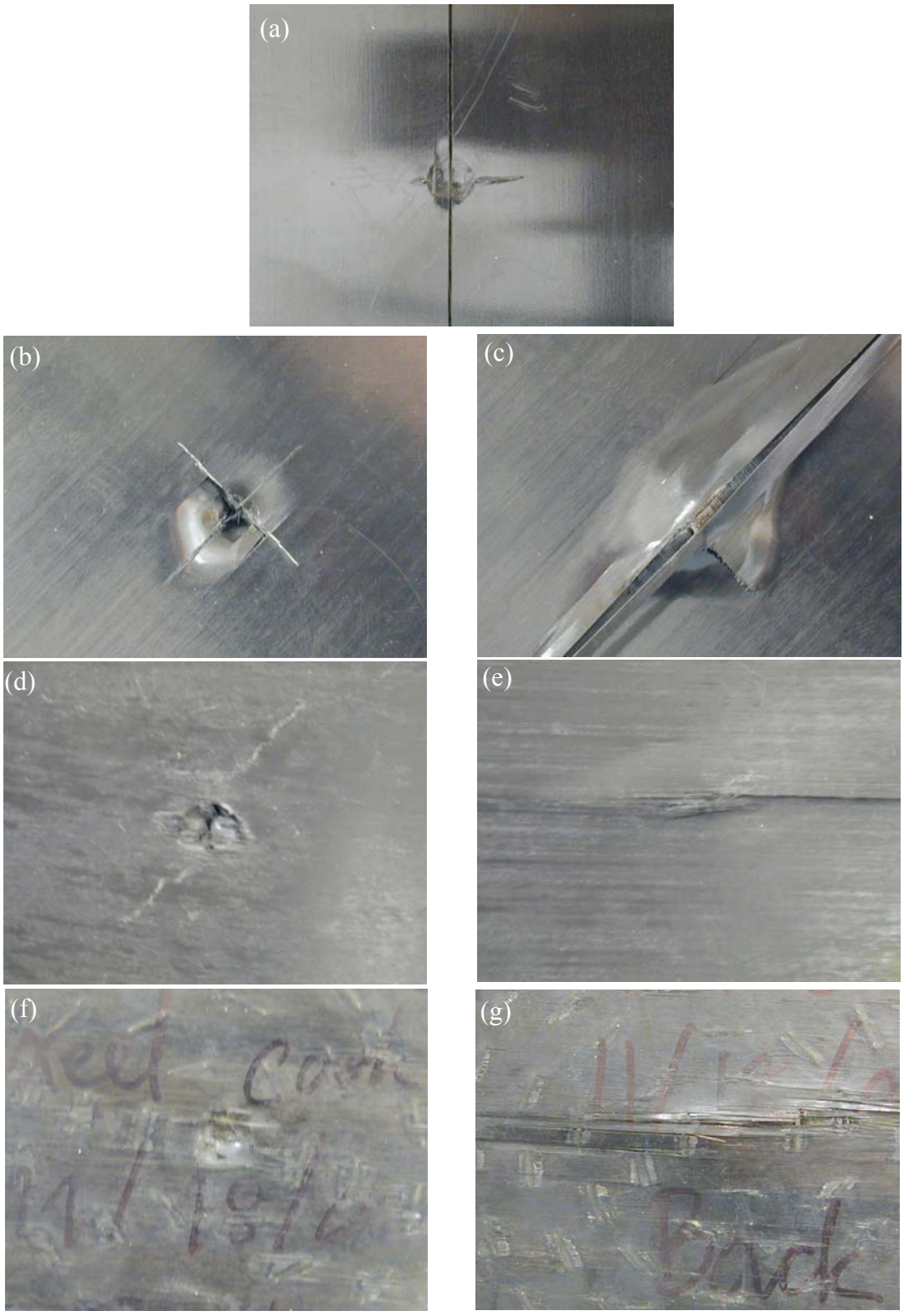

Figure 20. Damage patterns observed in the circular plate test. (a) 0° specimen. (b) and (c) Top and bottom sides of the ±45°, (d) and (e) top and bottom sides of the helicoidal specimen, (f) and (g) reinforced helicoidal specimen

4.4. Impact Tests

The impact test was employed to evaluate the effect of stacking geometry on the failure resistance of the specimen under dynamic loading conditions. In this experiment a striker propelled from an air-gun collided with the specimen normal to the plane of the fibers. It is difficult to obtain real-time information on the evolution of damage in this test configuration. This requires a diagnostic technique such as shadow moiré in conjunction with a high speed camera to capture back surface deflections as a function of time. Instead, post-test analysis of the damage was performed to compare the response of the different specimens. There was no particular reason to evaluate the unidirectional composite specimen, since this would provide a matrix dominated response. Therefore, the impact test performed only on the ±45° specimen and the helicoidal specimen.

The striker used in the impact experiments is shown in Figure 21; it was made of a polycarbonate (PC) rod, two inches in diameter and four inches long with a blunted conical tip made of solid steel attached to the front end. This striker was loaded into the barrel of an air-gun and launched by air pressure. In this air-gun, the striker was propelled using an air pressure of 80 psi; the speed of the striker before hitting with the laminate was measured to be 55 m/s corresponding to impacting energy 732 J.

The arrangement for applying the impact load is also shown schematically in Figure 21. In order to isolate damage occurring at the impact site from long term damage from stress accumulation at support points, the specimen was simply hung by a string in front of a catcher tank. The tank was filled with foam and clay to decelerate the specimen softly for recovery and observation of the impact induced damage. The normal to the specimen surface

was aligned to be along the axis of the gun barrel to ensure normal impact on the plate. The speed of striker was determined from a record of the time required for passing the distance between two light beams.

Figure 22 shows the back side of the ±45° specimen after impact failure. In this test the striker was propelled using an air pressure of 80 psi; the speed of the striker before hitting with the laminate was measured to be 55 m/s corresponding to impacting energy 732 J. After impact half the length of striker had penetrated through every layer of the laminate and the striker was embedded in the composite. The impacting force created the cross cracks along the ±45° fiber direction and totally delaminated every layer; a petaling failure can be seen in the close-up picture in Figure 22.

Next, the specimen with helicoidal stacking geometry was impacted under the same condition. The post-test view of the laminate is shown in Figure 23. Unlike in the ±45°

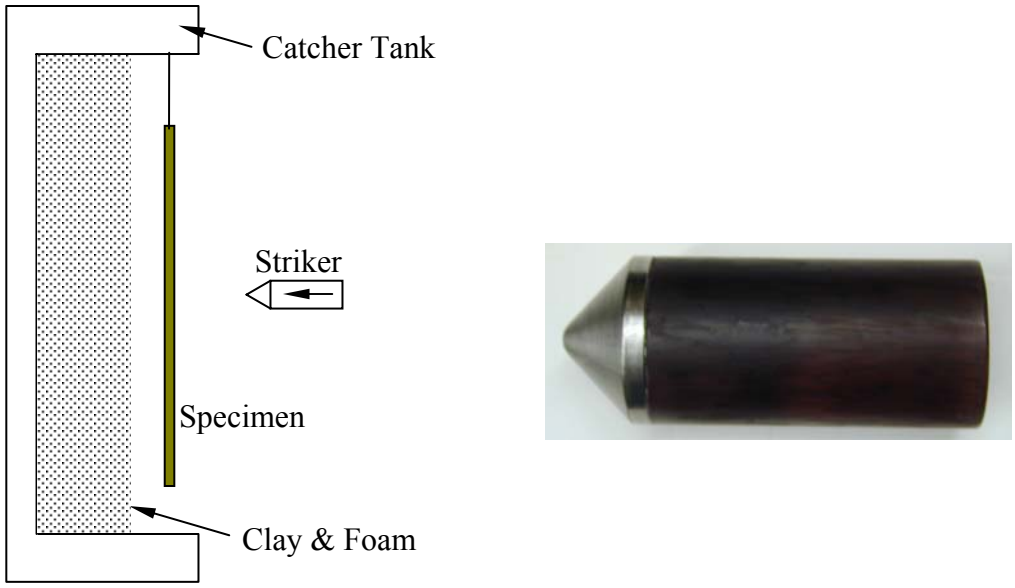

Figure 21. Impact test arrangement. Striker used in the impact tests is shown on the right. Conical tip was made of steel and the pusher was made of polycarbonate. Diameter 2 in.

specimen, the damage in this specimen was localized to the region of the impact. On the front side – the impact side, there was a small circular indentation caused by the striker tip and on the back side there were matrix cracks parallel to the fiber direction and delamination of the first layer was observed. The specimen was then sectioned and the delamination of the interior layers was verified. In spite of this, viewed in contrast to the observations on the ±45° specimen, we concluded that this helicoidal specimen was far below the penetration threshold.

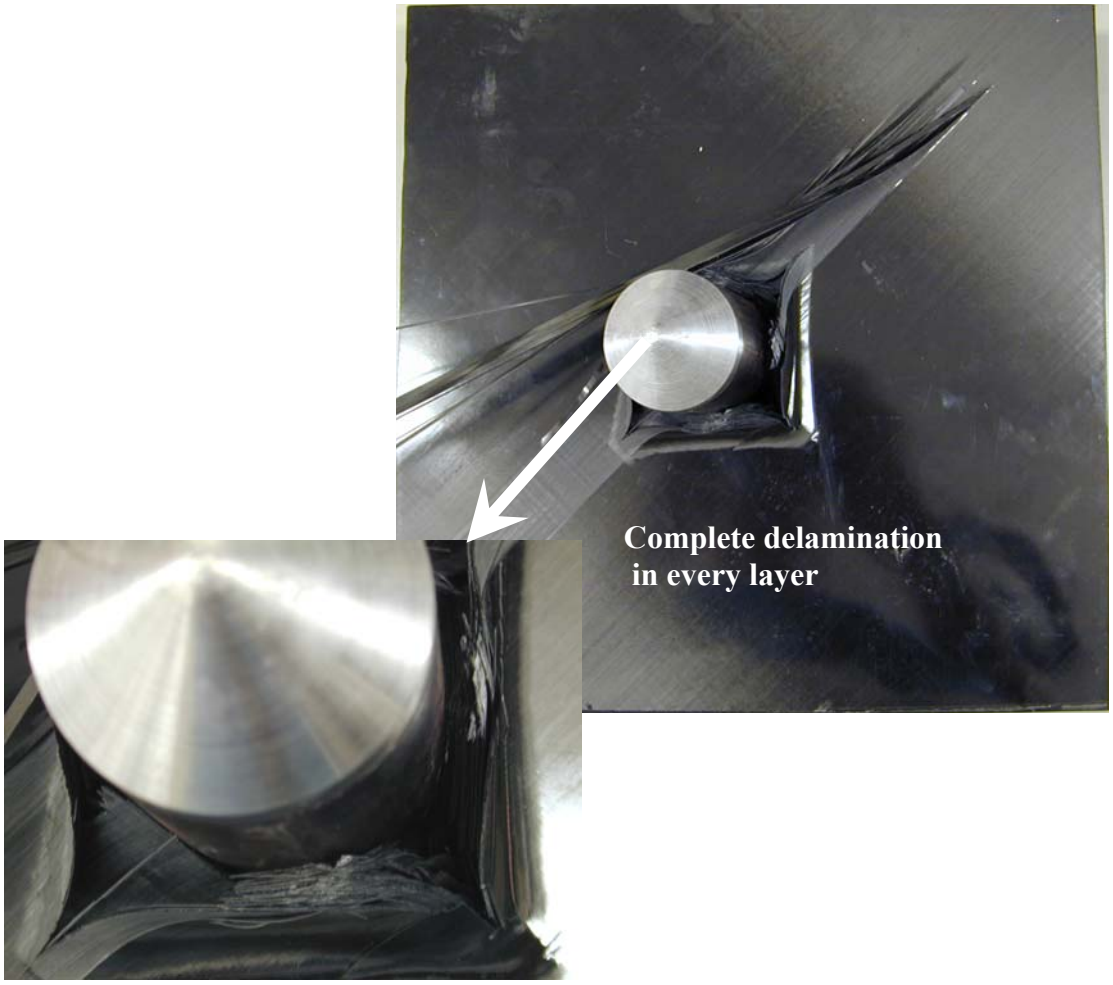

Figure 22. Back side of the ±45º specimen after the impact test.

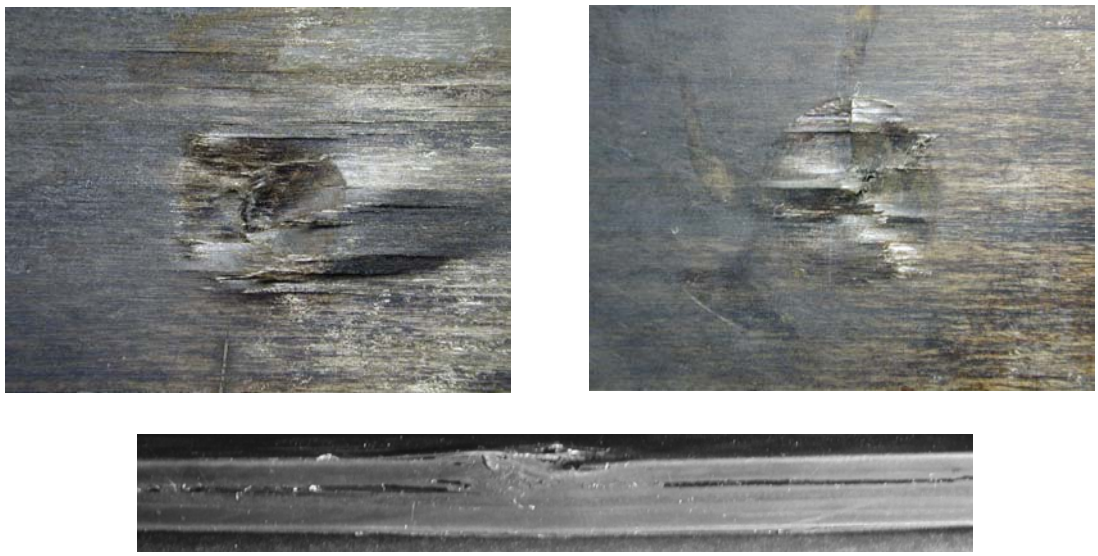

Figure 23. (a) and (b) Impact side of the helicoidal specimen after the impact test; the impact speed was 55 m/s. (c) Thickness section of the plate showing localized damage at the impact point and delamination along a specific layer.

Encouraged by this increase in the penetration resistance, we attempted to perform additional tests at higher impact speeds. Since we were at the limit of the air-gun capacity, increasing the projectile speed was only possible by making the PC backing on the striker to be hollow. This reduced the mass by 39% and enabled the projectile speed to increase from 55 m/s to 60.5 m/s. A similar damage pattern was observed as indicated in Figure 23b.

5. CONCLUSION

In an attempt to design composite specimens with improved mechanical properties, a new design based on a helicoidal architecture for the lay-up was considered. The motivation for this is derived from analysis of the state of stress in composite specimens with different fiber architectures. Finite element analysis showed that laminates that have an abrupt change in fiber orientation across layers also tend to have a higher interlaminar stress due to the mismatch of elastic properties; in contrast, for the helicoidal arrangement, the gradual change in in-plane properties in each layer results in lower interlaminar shear stresses. Therefore, a helicoidal composite was manufactured using a standard hand lay-up process. In addition, in order to improve the delamination resistance, reinforcement in the thickness direction was generated though the use of staples placed in a periodic arrangement.

Helicoidal composites were manufactured with 40 layers built on the following stacking arrangement: $[180/170/160/150/140/130/120/110/100/90/80/70/60/50/40/30/20/10/(0)2]_S$. The prepreg carbon-fiber epoxy NCT304-1 supplied from Newport Adhesives and Composites, Inc. in the form 36 inches wide continuous roll was used to prepare the specimens. Through-thickness reinforcement was provided in some of the specimens by the stapling with stainless steel staples. The specimens were cured through the manufacturer's recommended temperature and pressure cycle in an autoclave.

Different kinds of tests were performed in order to characterize the helicoidal composite: the standard tension test was performed to determine the stiffness and strength properties; the plate bending test and impact test were performed on circular plates to evaluate structural response; the three-point bending test was performed to evaluate the effect of interlaminar

shear stresses, and finally, the double cantilever beam test performed to evaluate the fracture toughness. Moreover, the finite element analysis software ABAQUS was used to simulate the deformation of the specimen in some of the tests and used to compare with the experimental results.

It is found that the specimen with helicoidal stacking sequence has better debonding resistance and improved damage tolerance. In a tensile test, it is shown that the helicoidal architecture results in higher energy absorption due to limits on the development of transverse cracks. In the circular plate test, the helicoidal specimen shows the highest load and energy absorption. In the impact test, it shows the highest penetration resistance. The reason for this behavior is that the different fiber orientations prevent continuous matrix cracking and link-up and therefore dissipate energy in every fiber direction. Some specimens with through-thickness reinforcement were manufactured and characterized. The reinforced laminate presents higher load carrying capacity, better delamination resistance and a graceful failure.

Although the many accomplishments in this work have created some understanding of helicoidal composites, there are still unanswered questions. In generating a more complete understanding of this material, further experiments and analysis have to continue in order to design and create the optimum structures with better quality in the future. Research in this field must be continued to obtain a final conclusion on the layer gradation, prestressing, and through-thickness reinforcement.

6. REFERENCES

T. Apicharttabrut, and K. Ravi-Chandar, 2003, Impact response of helicoidal composites, Report 03-04, Center for Mechanics of Solids, Structures and Materials, The University of Texas at Austin.

Y.A. Bahei-El-Din, and G.J. Dvorak, 1980, *Journal of Applied Mechanics*, 47, 827-832.

Y.A. Bahei-El-Din, M.A. Zikry, A.M. Rajendran, 2003, Impact-induced deformation fields in 3D cellular woven composites, *Composites: Part A*, **34**, 765–778.

D.J. Barrett. 1996, The mechanics of z-fiber reinforcement, *Journal of Composite Structures*, **36**, 23-32.

J.N. Baucom and M.A. Zikry, 2003, Evolution of failure mechanisms in 2D and 3D woven composite systems under quasi-static perforation, *Journal of Composite Materials*, 37, 1651-1674.

H. Chai, W.G. Knauss and C.D. Babcock, 1983, Observation of damage growth in compressively loaded laminates," Experimental Mechanics, 23, 329-337.

H. Chai, C.D. Babcock and W.G. Knauss, 1981, One dimensional modelling of failure in laminated plates by delamination buckling, *International Journal of Solids and Structures,* **17,**, 1069-1083.

H.Y. Choi, R. J. Downs and F.K. Chang, 1991a, A new approach toward understanding damage mechanisms and mechanics of laminated composite due to low-velocity impact: Part I-Experiments, *Journal of Composite Materials*, **25**, 992-1011.

H.Y. Choi, R.J. Downs and F.K. Chang, 1991b, A new approach toward understanding damage mechanisms and mechanics of laminated composite due to low-velocity impact: Part II-Analysis, *Journal of Composite Materials*, **25**, 1012-1038.

R.M. Christensen and S.J. DeTeresa, 1992, Elimination/minimization of edge-induced stress singularities in fiber composite laminates, *International Journal of Solids and Structures,* **29**, 1221-1231.

F. Collombet, J. Bonini, and J.L. Lataillade, 1996, A three-dimensional modelling of low velocity impact damage in composite laminates. *International Journal of Numerical Methhods in Engineering*, **39**, 1491–1516.

Giraud-Guille (1988) Twisted plywood architecture of collagen fibrils in human compact bone osteons, *Calcified Tissue International*, **42**, 167-180.

P.H. Geubelle and J.S. Baylor, 1998, Impact-induced delaminating of composites: a 2D simulation, *Composites Part B*, **29B**, 589-602.

C. Guo and C.T. Sun, 1998, Dynamic mode-I crack-propagation in a carbon/epoxy composite, *Composites Science and Technology*, **58**, 1405-1410.

H.M. Hsiao, I.M. Daniel and R.D. Cordes, 1998, Dynamic compressive behavior of thick composite materials. *Experimental Mechanics*, **38**, 172-180.

D. Hull, **An Introduction to Composite Materials**, Cambridge University Press, Cambridge 1981.

J.W.Joo and C.T.Sun 1992, A failure criterion for laminates governed by free edge interlaminar shear stress, *Journal of Composite Materials*, **26**, 1510-1522.

S. Kyriakides, R. Ascularatne, E.J. Perry and K.M. Liechti, 1995, On the compressive failure of fiber reinforced composites, *International Journal of Solids and Structures*, **32**, 689-732.

S.-W.R. Lee and C.T. Sun, 1993, Dynamic-penetration of graphite/epoxy laminates impacted by a blunt-ended projectile, *Composites Science and Technology*, **49**, 369-380.

J. Lambros and A.J. Rosakis, 1997, Dynamic crack initiation and growth in thick unidirectional graphite/epoxy plates, *Composites Science and Technology*, **57**, 55-65.

L.B. Lessard, O.P. Eilers and M.M. Shokreih, 1997, Modification of the three-rail shear test for composite materials under static and fatigue loading, *Composite Materials: Testing and Design, Thirteenth Volume*, ASTM STP 1242, S.J. Hooper, Ed., American Society for Testing and Materials, 217-233.

W.J. Liou, 1997, Impact analysis of laminated composite plates with statical indentation laws, *Journal of Computers and Structures*, **62**, 817-829.

T.-J. Lu and J.W. Hutchinson, 1995, Role of Fiber Stitching in Eliminating Transverse Fracture in Cross-Ply Ceramic Composites, *Journal of American Ceramic Society*, **78**, 251-253.

A.P. Mouritz, K.H. Leong and I. Herszberg, 1997a, A review of the effect of stitching on the in-plane mechanical properties of fiber-reinforced polymer composites, *Composites Part A*, **28A**, 979-991.

A.P. Mouritz, J. Gallagher and A.A. Goodwin, 1997b, Flexural Strength and Interlaminar Shear Strength of Stitched GRP Laminates Following Repeated Impacted, *Journal of Composites Science and Technology*, **57**, 509-522.

A. P. Mouritz, M.K. Bannister, P.J. Falzon and K.H. Leong, 1999, Review of applications for advanced three-dimensional fiber textile composites, *Composites Part A*, **30**, 1445-1461.

A.C. Neville, 1993, Biology of fibrous composites: development beyond the cell membrane, Cambridge University Press.

T.L. Norman and C.T. Sun, 1993, Delamination Growth in Composite Lmiantes with Adhesive Strips Subjected to Static and Impact Loading, *Journal of Composites Sciences and Technology*, **46**, 203-211.

T.K. O'Brien, Characterizatino of delamination onset and growth in a composite laminate, in *Damage in Composite Materials*, ASTM STP 775, ed. K.L. Riefsnider, 140-167.

T.K. O'Brien, 1997, Composite interlaminar shear fracture toughness G_{IIc}: Shear measurement or sheer myth? US Army Research Laboratory Technical Report 1312.

N.J. Pagano, 1978, Free edge stress fields in composite laminates, *International Journal of Solids and Structures,* **14,**, 401-406.

L.A. Pilato and M.J. Michno, 1994, **Advanced Composite Materials**, Springer-Verlag, Berlin.

K. Ravi-Chandar and W.G. Knauss, Dynamic crack tip stresses under stress wave loading – A comparison of theory and experiment. *International Journal of Fracture*, 1982, **20**, 209-222.

K. Ravi-Chandar, Dynamic shear crack propagation, Proceedings of the 10th International Conference on Fracture, December 2001.

K.L. Rugg, B.N. Cox, K.E. Ward and G.O. Sherrick, 1998, Damage mechanisms for angled through-thickness rod reinforcement in carbon-epoxy laminates, *Composites Part A*, **29A**, 1603-1613.

K.L. Rugg, B.N. Cox and R. Massabo, 2002, Mixed mode delamination of polymer composite laminates reinforced through the thickness by z-fibers, *Composites Part A*, **33**, 177-190.

G.A. Schoeppner and S. Abrate, 2000, Delamination threshold loads for low velocity impact on composite laminates, *Composites Part A*, **31A**, 903-915.

C.R. Schultheisz and A.M. Waas, 1996, Compressive failure of composites, Part I: Testing and micromechanical theories. *Progress in Aerospace Sciences*, **32**, 1-42.

A.P. Suvorov and G.J. Dvorak, 2001a, Optimized fiber prestress for reduction of free-edge stresses in composite laminates, *Internatinal Journal of Solids and Structures*, **38**, 6751-6786.

A.P. Suvorov and G.J. Dvorak, 2001b, Optimal design of prestressed laminate/ceramic plate assemblies, *Meccanica*, **36**, 37-109.

C.T. Sun, 1993, Inelastic properties of composites, in Materials Science and Engineering, A comprehensive Treatment, Vol 13: Structure and Properties of Composites, VCH, Weinheim.

S.R. Swanson, 1992, Limits of quasi-static solutions in impact of composite structures, *Composites Engineering*, **2**, 261–267.

S.R. Swanson, 1997, **Introduction to Design and Analysis with Advanced Composite Materials**, Prentice Hall, Upper Saddle River.

J. Tao and C.T. Sun, 1998, Influence of ply orientation on delamination in composite laminates, *Journal of Composite Materials*, **32**, 1933-1947.

S. Timoshenko, 1940, Theory of Plates and Shells, McGraw Hill, Inc., 1940.

J.L. Tsai, C. Guo and C.T. Sun, 2001, Dynamic delamination fracture toughness of unidirectional polymeric composites, *Composites Science and Technology*, **61**, 87-94.

A.M. Waas and C.R. Schultheisz, 1996, Compressive failure of composites, Paret II: Experimental studies, *Progress in Aerospace Sciences*, **32**, 43-78.

J.M. Whitney and R.J. Nuismer, 1974, Stress fracture criteria for laminated composites containing stress concentrations, *Journal of Composite Materials*, **8**, 254.

Z. Yang and C.T. Sun, 2000, Interlaminar fracture toughness of a graphilte/epoxy multidirectional composite, *Journal of Applied Mechanics*, **122**, 428-433.

S. Zheng and C.T. Sun, 1995, A double-plate finite-element model for the impact-induced delamination problem, *Composites Science and Technology*, **53**, 111–118.